Progress in Neurobiology 225 (2023) 102448

Contents lists available at ScienceDirect

Progress in Neurobiology

journal homepage: www.elsevier.com/locate/pneurobio

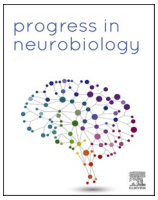

PolyQ length-dependent metabolic alterations and DNA damage drive human astrocyte dysfunction in Huntington's disease

Jenny Lange [a], Olivia Gillham [b,d,1], Michael Flower [a,1], Heather Ging [a], Simon Eaton [b], Sneha Kapadia [a], Andreas Neueder [c], Michael R. Duchen [d], Patrizia Ferretti [b,2], Sarah J. Tabrizi [a,e,*,2]

[a] Huntington's Disease Centre, Department of Neurodegenerative disease, UCL Queen Square Institute of Neurology, University College London, WC1N 3BG, UK
[b] Stem Cell and Regenerative Medicine Section, UCL Great Ormond Street Institute of Child Health, WC1N 1EH3, UK
[c] Department of Neurology; Ulm University, 89081 Ulm, Germany
[d] Department of Cell and Developmental Biology and Consortium for Mitochondrial Research, UCL, Gower St, WC1E 6BT, UK
[e] Dementia Research Institute at UCL, London WC1N 3BG, UK

ARTICLE INFO

Keywords:
Huntington's disease
Pluripotent stem cells
Astrocytes
Metabolism
DNA damage

ABSTRACT

Huntington's Disease (HD) is a neurodegenerative disease caused by a polyglutamine (polyQ) expansion in the Huntingtin gene. Astrocyte dysfunction is known to contribute to HD pathology, however our understanding of the molecular pathways involved is limited. Transcriptomic analysis of patient-derived PSC (pluripotent stem cells) astrocyte lines revealed that astrocytes with similar polyQ lengths shared a large number of differentially expressed genes (DEGs). Notably, weighted correlation network analysis (WGCNA) modules from iPSC derived astrocytes showed significant overlap with WGCNA modules from two post-mortem HD cohorts. Further experiments revealed two key elements of astrocyte dysfunction. Firstly, expression of genes linked to astrocyte reactivity, as well as metabolic changes were polyQ length-dependent. Hypermetabolism was observed in shorter polyQ length astrocytes compared to controls, whereas metabolic activity and release of metabolites were significantly reduced in astrocytes with increasing polyQ lengths. Secondly, all HD astrocytes showed increased DNA damage, DNA damage response and upregulation of mismatch repair genes and proteins. Together our study shows for the first time polyQ-dependent phenotypes and functional changes in HD astrocytes providing evidence that increased DNA damage and DNA damage response could contribute to HD astrocyte dysfunction.

1. Introduction

Huntington's Disease (HD) is a fatal, neurodegenerative disorder caused by a polyglutamine (polyQ) expansion in exon 1 of the Huntingtin gene (Ross and Tabrizi, 2011). Unaffected individuals carry < 36 CAG repeats, whilst individuals with > 40 CAG will develop HD (Andrew et al., 1993). Symptoms of HD include chorea, psychiatric symptoms and dementia. Despite ubiquitous expression of the mutant (m)HTT protein, striatal medium spiny neurons and cortical pyramidal neurons are subject to early, selective neurodegeneration whilst other subpopulations are relatively spared (Johnson et al., 2020; Rosas et al., 2008). In addition to neuronal loss, astrocytes have been implicated in HD disease progression (Khakh et al., 2017; Palpagama et al., 2019). Astrocytes are the most numerous glial cells in the human brain and are involved in many crucial functions of the nervous system, including maintaining homeostasis, providing neuronal support, synaptic modulation and immune response (Liddelow and Barres, 2017; Singh and Abraham, 2017; Vainchtein and Molofsky, 2020). Increased GFAP reactivity of astrocytes, a hallmark of astrocyte activation, has been reported in post-mortem HD human brains and its extent appeared to correlate with the severity of degeneration of striatal neurones (Rueb et al., 2015; Vonsattel et al., 1985). Despite increased GFAP reactivity, HD astrocytes do not seem to present classical activated phenotypes. Neither a clear neurotoxic (A1 subtype) or neuroprotective (A2 subtype)

* Corresponding author at: Huntington's Disease Centre, Department of Neurodegenerative disease, UCL Queen Square Institute of Neurology, University College London, WC1N 3BG, UK.
E-mail address: s.tabrizi@ucl.ac.uk (S.J. Tabrizi).
[1] These authors contributed equally to the research.
[2] Joint senior authors

https://doi.org/10.1016/j.pneurobio.2023.102448
Received 5 September 2022; Received in revised form 3 February 2023; Accepted 24 March 2023
Available online 5 April 2023

phenotype has been observed by single and bulk RNA sequencing of mouse and human post mortem samples at various disease states (Benraiss et al., 2021; Diaz-Castro et al., 2019).

A potential role of DNA damage repair pathways in HD pathogenesis has been emerging. However, it has yet to be addressed whether human HD astrocytes are affected by a higher burden of DNA damage and/or a defective DNA damage response. Elevated DNA damage has been detected in human fibroblasts and blood cells from prodromal HD patients (Askeland et al., 2018; Castaldo et al., 2019; Maiuri et al., 2017) as well as in mouse models where it precedes protein aggregation (Maiuri et al., 2019). Genome wide association studies (GWAS) have identified several genes involved in the DNA mismatch repair (MMR) pathway as significant modifiers of HD age of onset and severity (Iyer and Pluciennik, 2021) by influencing somatic expansion of CAG repeats. Most notably, in affected brain regions including the cortex and striatum the number of CAG repeats expands progressively over time (Pinto et al., 2013; Shelbourne et al., 2007; Swami et al., 2009). Whilst somatic CAG expansion in vulnerable neurons is thought to drive age of onset in HD, it is not known to which extent astrocytes may be involved or are subject to MMR pathway dysregulation.

The majority of studies aimed at understanding how astrocytes are affected in HD have been carried out in mouse models (Chen et al., 2012; Dvorzhak et al., 2016; Polyzos et al., 2019; Tong et al., 2014; Wójtowicz et al., 2013). While HD animal models have aided our understanding of potential roles of astrocytes in disease pathogenesis, and suggested that defective astrocyte metabolism may cause or exacerbate neuronal dysfunction, they do not fully phenocopy the human disease (Benraiss et al., 2021). Human HD astrocytes derived from PSC (pluripotent stem cells), such as embryonic (ESC) or induced pluripotent stem cell (iPSC), have been shown to mirror some phenotypes observed in post-mortem human HD brains, but have yet to be extensively studied (Cho et al., 2019; Garcia et al., 2019). Interestingly, in co-cultures with healthy neurons, human HD astrocytes were found to reduce neuronal maturation and displayed impaired calcium modulation (Garcia et al., 2019). However, there are many crucial outstanding questions concerning human astrocyte behaviour with HD progression.

Here, we have used a series of isogenic or highly related human ESC- and IPSC-derived astrocytes ranging from 45Q to 180Q in order to examine common and polyQ length dependent phenotypes. Furthermore, this system allows us to examine cell autonomous phenotypes in astrocytes that are not driven by neuronal dysfunction. Our first aim was to identify common dysregulated genes and pathways in our human astrocytes (58Q, 69Q, 75Q, 125Q and 180Q) by bulk RNA sequencing, as to date no RNA expression data for IPSC-derived astrocytes is available. Our second aim was to establish whether the extent of HD astrocyte reactivity and metabolic activity, which is often altered concomitantly with astrocyte activation, was differently affected by polyQ length by gene expression analysis and metabolic assays. Finally, we wanted to establish whether DNA damage may play a role in HD astrocyte dysfunction by assessing cell death, oxidative stress, double strand breaks and DNA damage response. Hence, we investigated expression of MMR genes and proteins, as well as somatic expansion in HD astrocytes.

2. Methods

2.1. Cell lines

RUES ESC lines (20Q, 56Q) were derived and provided by Prof. Ali Brinvalou's Laboratory (Rockefeller University) (Conforti et al., 2020). The IsoHD ESC lines comprising lines with 30Q, 45Q and 81Q were generated and validated as described in (Ooi et al., 2019) and kindly provided by Dr. Mahmoud Pouladi. The QS IPSC series (22Q, 58Q, 69Q and 75Q) and 125Q IPSC lines were generated at University College London Queen Square as previously described (Goold et al., 2021; Lange et al., 2021b). 180Q IPSCs were provided by Dr. Gabriel Balmus and generated as described by (Tidball et al., 2016). The 19Q control line (Lange et al., 2021a) was generated by Dr Olivia Gillham according to (Hawkins et al., 2016) and used as an additional control alongside the QS22 for 125Q and 180Q lines.(Table 1).

2.2. Cell culture

PSC lines were maintained in Essential 8 Media (Thermo Fisher Scientific) on Geltrex coated plates (1 % in DMEM –F12, Gibco Life Technologies) and we passaged at ~ 80 % confluency using RELESR according to manufacturer's instructions.

2.2.1. Neural Induction and astrocyte differentiation

Neural progenitor fate was induced as previously described (Fitz-Patrick et al., 2018; Lange et al., 2021b). Briefly, IPSCs were passaged into U-bottom 96 well plates at a density of 1×10^4 cells per well in neural induction media (NIM) supplemented with ROCKi. Daily media changes were performed until day 6 when clusters were plated onto laminin coated 6-well plates. Neural rosettes were picked after a further 4 days, spun at 200 g for 5 min and plated onto laminin coated 6 well plated in human neural stem cell media (Lange et al., 2021a; Vagaska et al., 2020). Neural progenitor like cells (NPCs) were expanded for at least 5 passages before astrocyte fate was induced by passaging NPCs using Accutase into T25 flasks in astrocyte media. As HTT plays a role in neurodevelopment, and this study aimed to detect early phenotypes, an early differentiation time point, 28 days (Lange et al., 2021a), was chosen to assess astrocyte function. Astrocytes were plated for immunocytochemistry, cell viability or functional experiments onto 96 well plates at 1×10^4 cell/cm^2. Alternatively, astrocytes were harvested and pelleted for western blot analysis after 28 days differentiation.

2.3. Cell viability assay

Cell viability under basal conditions was quantified using propidium iodide (PI) as previously described (Lange et al., 2021a). Two hours prior to imaging, astrocytes were given a full medium change containing PI (Invitrogen, final concentration 5 μg/ml) and Hoechst.

2.4. Metabolic assays

For all functional assays, astrocytes were plated at a density of 1×10^4 cells/well in 96 well plates. Subsequent experiments were carried out 48 h after plating. All experiments were carried out in a minimum of technical triplicates with three separate differentiations per cell line.

For ATP and MTT assays, astrocytes were plated in duplicates across

Table 1
ESC- and IPSC- cell lines.

	polyQ length	Name	Cell Type	Origin	
Rues20	20 (Control)	RUES	ESC	Rockefeller University	Isogenic Pair
Rues56	56				
Sues30	30 (Control)	IsoHD	ESC	Singapore University	Isogenic Series
Sues45	45				
Sues81	81				
QS22	22 (Control)	QS	iPSC	Queen Square University College London	Highly genetic related series (mother and three affected siblings)
QS58	58				
QS69	69				
QS75	75				
19Q	19 (Control)		iPSC	Institute of Child Health	Additional control line for non-isogenic lines
125Q	125		iPSC	Queen Square	No isogenic control
180Q	180		iPSC	HD Consortium	No isogenic control

2 plates, where the second plate was fixed and used to obtain cell counts using Hoechst for each well to normalise the assay. For all other assays, plates were fixed after supernatant collection and cell counts were performed using Hoechst on an Opera Phenix high content screening system (PerkinElmer Cellular Technologies).

Metabolic activity was measured using an MTT assay as previously described (Lange et al., 2021a). Briefly, MTT 3-(4, 5-dimethylthiazol-2-yl)− 2,5-diphenyltetrazolium bromide was added to astrocytes for two hours after which cells were washed with PBS. 200 µl of Dimethyl sulfoxide (DMSO) were added per well and 100 µl were taken for an absorbance read out at 595 nm on a Tecan microplate reader (Life Sciences).

Cellular ATP content was examined using a CellTiter-Glo ATP assay (Promega). 100 µl of CellTiter-Glo reagent was added to astrocytes in 100 µl supernatant, the plate was shaken for 5 min and incubated at room temperature after a further 30 min. Luminescence was measured using a Tecan microplate reader.

2.5. Glutamate uptake

To measure glutamate uptake, supernatant was removed from astrocyte cultures and replaced with fresh astrocyte media containing 50 µM Glutamate. After 30 min, supernatant was collected and the amount of glutamate measured using a Glutamate assay kit (Cell Biolabs) according to manufacturer's instructions and as previously described (Birger et al., 2019).

2.6. Lactate and cholesterol secretion

48 h after plating, a full media change was performed and after two hours supernatant was collected to measure Lactate and Cholesterol secretion. A Lactate Detection kit (Promega) and a Cholesterol-Glo kit (Promega) was used according to manufacturer's instructions to measure lactate and total cholesterol (including Cholesterol Ester) respectively.

2.7. Glucose oxidation

Glucose metabolism was measured using gas chromatography isotope-ratio mass spectrometry (GC-IRMS) as previously described (Lange et al., 2021a). Astrocytes were plated in 6-well plates at 9×10^4 cells/well and after 48 h a full medium change was performed with experimental medium (glucose free DMEM with 15 mM HEPES, 2.9 mM sodium bicarbonate, 2 mM L-glutamine, 0.5 mM sodium pyruvate and 21.5 µM phenol red with 3 mM D-glucose added). After 20 h, experimental medium was removed and cells were washed with PBS, 3 ml experimental DMEM with 3 mM [U-^{13}C] Glucose were added per well. Wells were sealed with a 3 ml layer of heavy mineral oil to prevent loss of $^{13}CO_2$. 100 µl of supernatant were collected at 0 and 24 h and stored in rubber-sealed Exetainer™ vials (Labco Ltd, Ceredigion, UK) at − 20 C. Once thawed, 100 µl of 1 M hydrochloric acid was added to release CO_2. Samples were centrifuged at 500 g for 30 s and analysed on a GasBench II linked to a Thermo Delta-XP isotope-ratio mass sprectrometer (Thermo-Finnigan, Bremen, Germany).

2.8. Mitochondrial oxygen consumption

Mitochondrial oxygen consumption rate (OCR) was measured using a Seahorse XFe96 Analyzer (Agilent Technologies), in order to assess mitochondrial function using Agilent Seahorse XFe96 FluxPaks (Agilent Technologies, 102416-100). Astrocytes were seeded 48 h prior to analysis at 2×10^4 cells per well, with at least 14 technical replicate wells seeded for each line per run. Assay cartridges were hydrated prior to the assay, by adding 200 µl Seahorse Calibrant per well and incubating at 37C for 24–48 h. On the day of each assay, Seahorse XF DMEM medium (Agilent Technologies, 103575-100) was freshly supplemented with 1 mM pyruvate, 2 mM L-glutamine and 10 mM D-glucose. Cells were carefully washed using 200 µl of this complete Seahorse XF DMEM per well, then a fresh 150 µl medium was added to each well followed by incubation for 1 h at 37C in a CO_2-free LEEC compact incubator. The mito-stress test was carried out according to manufacturer's instructions. Oligomycin was used at a final concentration of 2.5 µM, FCCP was used at two sequential dilutions of 0.75 µM and 1.5 µM to ensure the optimal concentration was used for each cell line, then Antimycin-A was used at a final concentration of 2.5 µM. Following the assay, Hoechst 33342 was added to each well at a final concentration of 2 µg/ml and incubated with cells for 20 min. Cells were then imaged and counted using an ImageXpress High Content Screening System, and cell numbers used to normalise OCR per well for analysis using Agilent Technologies Wave 2.6.1 software.

2.9. Immunocytochemistry

Astrocyte cultures were fixed on day 30 with 4 % PFA for 15 min at room temperature, washed 3 times in PBS and stored in PBS containing 0.02 % sodium azide. After permeabilization with 0.02 % Triton for 15 min, fixed astrocytes were incubated in blocking solution (1 % BSA, 10 % normal goat serum in PBS) for one hour at room temperature. Primary antibodies (Table 2) in 1 % BSA in PBS were added overnight and kept at 4 C. After 5 washes in PBS, secondary antibodies (Alexa 488, Alexa 594, Alexa 633, Invitrogen) and Hoechst in PBS containing 1 % BSA were added for 1 h at room temperature. Following a further 5 washes, fixed astrocytes were kept at 4 C in 0.02 % sodium azide in PBS until imaging.

2.10. High content imaging

High content imaging was carried out on the Opera Phenix high content screening system (PerkinElmer Cellular Technologies) running a Harmony user interface software as previously described (Ref) with adjustments made for astrocytes. All images were taken with binning set at 2 and 30 fields of view per well in 6 replicate wells per condition. Well set height for all astrocyte cultures was optimised by generating a Z-stack for each condition and set at 1 µm. Images for viability (PI/Hoechst) and cell counts (Hoechst) were taken with a 10x objective, all other images were taken with a 25x objective. Images were processed as previously described (Lange et al., 2021b), and results were exported to excel and analysed in GraphPad Prism8.

2.11. Protein extraction

Astrocytes were harvested from T25 flasks using Tripzean (per manufacturers instructions), spun down and resuspended in RIPA buffer. Cell lysates were then kept at 4 C for 30 min, spun at 10,000 g for 15 min and supernatant was collected for quantification of protein levels

Table 2
Primary antibodies used for immunocytochemistry.

	Species	Dilution	Catalogue Number	Supplier
53BP1	rabbit	1:200	ab21083	Abcam
8-OhDG	mouse	1:200	Sc-66036	Santa Cruz
Aquaporin4	rabbit	1:500	ab125049	Abcam
EM48	mouse	1:100	MAB5374	Millipore
GFAP	chicken	1:1000	ab4674	Abcam
Glutamine Synthetase	mouse	1:100	Sc-74430	Santa Cruz
Ki67	mouse	1:400	550609	BD Biosciences
Nf-kB	rabbit	1:500	8242	Cell Signaling Technologies
SOX2	rabbit	1:200	Ab97959	Abcam
Vimentin	mouse	1:200	MA3–745	Thermo Fisher Scientific
yH2AX	rabbit	1:500	ab11174	Abcam

(BCA assay kit, Thermofisher). Samples were kept at − 80 until use.

2.12. Western blotting

Western Blots were run in a Xcell Sure Lock Mini-Cell (Life Technologies) using the NUPAGE system. For low molecular weight proteins (15–200kDA) samples were run on a 3–12 % Tris Bis Gel, higher molecular weight proteins were run on a 3–8 % Tris Acetate gel. Protein gels were run at 75 V for 30 min and for a further hour at 150 V. Gels were transferred onto a nitrocellulose membrane (low molecular weight, Tris Bis gel) or PVDF membrane (higher molecular weight, Tris-Acetate gel) at 35 V for two and a half hours. Membranes were incubated in Intercept Blocking Buffer (Licor) for 1 h at room temperature and incubated in primary antibody (Table 3) in blocking buffer overnight at 4 C. Membranes were washed in PBS-T three times and incubated in secondary antibodies (LICOR, donkey anti rabbit 680 and donkey anti mouse 800, 1:10000) for one hour at room temperature. Following a further 3 washes in PBS-T, proteins were visualised using an Odyssey western blot system (LI-COR).

2.13. Quantitative PCR

RNA was extracted using an RNEasy minikit (Qiagen) according to manufacturer's instructions. cDNA was synthesised using Superscript IV (Thermo Fisher Scientific). 100 ng RNA per sample were added to 1 µl dNTPs (10 mM) and 1 µl random hexamers (100 ng/µl) and brought up to 13 µl with RNAse free water. Samples were heated to 65 C for five minutes, chilled on ice for one minute after which 4 µl 5x Superscript IV buffer, 1 µl Superscript IV Reverse Transcriptase, 1 µl DTT (100 mM) and 1 µl RNAse Inhibitor were added per sample. These were then cycled for 10 min at 23 °C, 55 °C and 80 °C before 1 µl RNAse H was added to each sample and incubated for 20 min at 37 °C. Samples were frozen until qPCR could be performed. 3.5 µl sample was added to 3.75 µl water, 7.5 µl TaqMan Fast Advanced Mastermix (Thermo Fisher Scientific) and 0.75 µl of probe for the gene of interest (Table 4) and housekeeper genes (ATP5B, UBC, EIF4; Thermo Fisher Scientific) in a 96 well plate and quantified in a QuantStudio 5 ProFlex system using the following conditions: 95 °C for 40 s, 40 cycles of 95 °C for 15 s and 60 °C for 30 s. Data obtained were analysed using the comparative cycle threshold method (ΔΔCt) (Schmittgen and Livak, 2008).

2.14. CAG repeat sizing

Fragment analysis was performed by PCR of the CAG repeat using the primers MFHDS3F 5'– 6FAM-CCATGGCGACCCTGGAAA-3' and MFHDS3R 5'-AGCGGGCCCAAACTCAC-3' with Amplitaq Gold 360 (Thermo). Products were resolved by capillary electrophoresis on a 3730XL Genetic Analyzer (ABI). Results were displayed using GeneMapper software (Thermo), and analysed using a custom R script, available at https://caginstability.ml. The rate of CAG expansion was modelled as a linear regression of CAG expansion on the number of days in culture. Expansion rates are compared by anova of a linear mixed effects model in R, with biological replicate as a random effects variable.

Table 3
Primary anitibodies used for Western blotting.

	Species	Dilution	Catalogue number	Supplier
53BP1	rabbit	1:500	ab21083	Abcam
Actin	mouse	1:5000	A5316	Sigma
Actin	rabbit	1:5000	Ab8227	Abcam
AKT	rabbit	1:1000	9272S	Cell Signaling Technologies
pAKT	rabbit	1:1000	4058L	Cell Signaling Technologies
ATM	rabbit	1:1000	ab36810	Abcam
pATM	mouse	1:1000	ab32420	Abcam
FAN1	sheep	1:2500	N/A	CHDI Foundation
MLH1	mouse	1:1000	51–1327GR	BD Biosciences
MSH2	rabbit	1:1000	D24B5	Cell Signaling Technologies
MSH3	mouse	1:1000	611930	BD Biosciences
MSH6	mouse	1:1000	610919	BD Biosciences
NEK1	mouse	1:100	SC398813	Insight Biotechnology
p53	mouse	1:100	SC-126	Insight Biotechnology
RAD51	rabbit	1:1000	ab133534	Abcam
γH2AX	rabbit	1:2500	ab11174	Abcam

Table 4
QPCR probes.

Gene	Catalogue number	Gene	Catalogue number
ADORA2A	HS00169123	MSH3	HS00989003
Aldh1l1	HS01003842	MSH6	HS00943000/HS00264721
ATP5B	HS00969569	Nestin	HS04187831
C3	HS00163811	PMS1	HS00922262
EIF4A2	HS00756996	PMS2	HS00241053
FAN1	HS00429686	S100A10	Hs00751478
HTT	HS00918174	S100b	HS00902901
IL-6	HS00174131	SDHA	HS00188166
MLH1	HS00979919	UBC	HS00824723
MSH2	HS00954125	VEGFA	HS00900055

2.15. RNA sequencing

RNA sequencing was performed as previously described (Lange et al., 2021a). Briefly, 100 ng of RNA per sample was used to generate RNA libraries by UCL Genomics. Each cDNA fragment was tagged with a sample specific sequence (index) and a unique molecular identifier (UMI). Samples were sequenced on the Illumina NextSeq 2000 that generated approximately 25 M reads/sample. Raw data was processed to remove poor quality base calls and contaminating Illumina adapter sequences. Reads that were shorter than 15 bases after trimming were discarded as these were considered too short to be mapped uniquely. Obtained reads were aligned to the human reference genome (GRCh38) with RNA Star. PCR duplicate reads were then removed using the mapping loci and the molecular identifier to ensure that a read is a true PCR duplicate. The raw count per transcript was then estimated. Additional quality control was performed to confirm that there was no excess ribosomal contamination. Transcripts per million (TPM) were obtained for 26486 genes and FASTQ sequencing data were further processed in SARTools. Normalised TPM values for all genes can be found in Supplementary Table 1.

For the QS series, differential expression analysis was performed on the 22Q isogenic control against 58Q, 69Q and 75Q separately. For non-isogenic lines differential expression analysis was performed on each of two control lines (22Q, 19Q) against each of non-isogenic HD lines (125Q, 180Q) separately using SARTools package (DESeq2 wrapper). The primary analysis in this report tested whether there was differential expression between each HD line and relevant control lines. This was done by combining the association p values for each gene using Brown's method which is essentially the Fisher's method for combining p values (Brown, 1975). The analyses were performed on three cell line comparisons, each HD astrocyte line versus healthy 22Q and 19Q; p values were Bonferroni corrected for three tests. This is conservative given that the disease groups are not independent. For comparison, p values were also combined using the Fisher's method (Dai et al., 2014) and the harmonic mean (Wilson, 2019). Log2fold change was combined by fixed effects meta-analysis to yield a standardised mean difference. These analyses were performed using a custom R script available on request.

Gene Ontology (GO) enrichment analysis was performed using ShinyGo v0.66 (bioinformatics.sdstate.edu/go/) for Biological Processes, Cellular Components and Molecular Function on up- and down-regulated DEGs with Benjamin-Hochberg p-value correction of FDR< 0.05 for statistical significance. We first examined up- and down-regulated GO terms for shared DEGs across all lines, and then the top up- and down-regulated GO terms for each HD line and extracted terms enriched in all HD lines.

Kyoto Encyclopedia of Genes and Genomes (KEGG) Pathway analysis for Biological Processes was performed using Selection by iterative pathway group and network analysis looping (SIGNAL: https://signal.niaid.nih.gov/) (Katz et al., 2021) in up and down-regulated genes with $p < 0.05$. Log2Fold Changes were used as cut off values (Medium Confidence Cutoff Value >2, High Confidence Cutoff Value >7) and pathways were considered significantly enriched if the FDR was < 0.05. ECM-receptor interaction pathway information was obtained from (Kanehisa and Goto, 2000).

Hallmark pathway analysis was conducted using the fgsea package in bioconductor. Pathways were downloaded from MSigDB. Normalised enrichment scores were plotted, with colour indicating adjusted p values with significance < 0.05.

Weighted correlation network analysis (WGCNA) was performed in R using the WGCNA package (Langfelder and Horvath, 2008). WGCNA compares expression of genes across multiple samples to define modules, which are clusters of highly interconnected genes, in an unbiased fashion. Intramodular connectivity is a measure of how co-expressed a gene is with respect to others in the same module; it can be considered a measure of each gene's module membership. The module eigengene (*E*) is the first principal component of each module, and represents the gene expression profile of that module; one can correlate *E* with traits, such as disease status and CAG repeat length, to determine the module significance. The 'hub gene' is the most central, or highly connected, gene within each module. We examined the top up- and down-regulated GO terms for each module in each HD line. WGCNA analysis was additionally performed on the HD post mortem data described by (Lin et al., 2016). Overlap analysis of WGCNA modules was performed on the following data sets: Lin et al., (2016), Diaz-Castro et al. (2019) and Hodges et al. (2006) as described by Neueder and Bates (2014). For the latter SRA files and accompanying meta-data were downloaded from the NCBI GEO database, accession number GSE79666. SRA files were converted to fastq files using fastq-dump v2.8.2 from the NCBI SRA-Toolkit (https://trace.ncbi.nlm.nih.gov/Traces/sra/sra.cgi?view=software). Fastq files were quality controlled with FastQC v0.11.5 (https://www.bioinformatics.babraham.ac.uk/projects/fastqc/). All files passed QC. The reads were aligned against Ensembl Homo sapiens GRCh38 release 90 using STAR aligner v2.5.3a (Dobin et al., 2013). Reads were quantified using salmon v0.8.2 (Patro et al., 2017). All subsequent analyses were conducted in R v3.4.1 and v3.4.3. Transcriptional dysregulation was computed using tximport v1.10.0 (Soneson et al., 2016) and DESeq2 v1.22.1 (Love et al., 2014) with HD status as the variable of interest. The normalised and transformed counts from the DESeq2 analysis were used to construct a weighted gene correlation network using WGCNA v1.61 (Langfelder et al., 2013; Langfelder and Horvath, 2008) as previously described (Neueder and Bates, 2014). Briefly, signed correlation matrices were constructed using robust correlation with maxPOutliers = 0.05. Power for the network construction was 13. Modules with a correlation of 80 % or more were merged. Scripts are available upon request.

Metabolic Reaction Enrichment analysis (MAREA) was performed in GALAXY, using MAREA4Galaxy (Damiani et al., 2020). Reaction Activity Scores (RAS) were calculated from TPM values for each DMD line and merged control lines using the Expression2RAS module. Here we used the HMRcore human metabolic network module which corresponds to the core model of central carbon metabolism (Damiani et al., 2020). The control RAS data set was then compared to each control line using the MAREA module. Differences between groups were considered significant if the p-value threshold determined by Kolmogorov-Smirnov test was < 0.01 and the threshold fold-change was > 1.2.

2.16. Statistics

For all quantification, each line was differentiated 3 times in independent experiments with a minimum of three technical repeats.

All statistical analysis (with the exception of RNA sequencing analysis) was carried out in Graphpad Prism 8. HD lines were compared to their isogenic control where available (RUES, SUES and QS) and in the case of the 125Q and 180Q IPSC lines were compared to 22Q and 19Q IPSC derived lines. Where appropriate either a student's t-test or two-way ANOVA with Bonferroni's multiple comparison's correction was carried out with a 95 % confidence interval and values with $p < 0.05$ were considered statistically significant. Statistical significance is indicated as * $p < 0.05$, * * $p < 0.01$, * ** $<p < 0.001$. All data is reported at mean ± SEM.

3. Results

3.1. RNA sequencing shows widespread transcriptional disruption in iPSC-derived HD astrocytes

We performed RNA sequencing on astrocytes derived from three highly related IPSC lines (58Q, 69Q, 75Q) and their isogenic control (22Q), as well as 125Q and 180Q IPSC lines which we compared to an additional control (22Q, 19Q). Differential Gene Expression (DEG) revealed a large number of up- and down-regulated genes in HD lines versus their respective controls (Supplementary Table 1), with a sizeable number of shared DEGs between astrocytes with similar polyQ lengths (Fig. 1a). We found 20 up-regulated genes and 34 down-regulated genes that were shared across all HD astrocytes (Fig. 1a,b, Supplementary Table 1b,c). Gene Ontology (GO) enrichment analysis performed on the shared genes revealed several significantly enriched GO terms for down-regulated biological processes and cellular components (Fig. 1c), which largely centred around synapses and synaptic transmission as well as nervous system development and neurogenesis.

We next performed GO analysis on all DEGs for each line and extracted significantly enriched GO terms that were shared across all lines (Fig. 1d); a complete table of all shared GO terms can be found in Supplementary Table 2. Consistent with GO analysis for shared genes in HD astrocytes, significantly down-regulated GO terms were highly related to neuron development, cellular signalling and synapses. Furthermore, the data suggests significant dysregulation of astrocytic contribution to synaptic activity. Notably, up-regulated genes linked to positive and negative regulation of metabolic processes were highly enriched in HD astrocytes, suggesting dysregulation of various aspects of astrocyte cellular metabolism (Fig. 1d, Supplementary Table 3). Binding of several molecules appears to be disrupted in HD astrocytes, with several terms in both up- and down-regulated molecular functions including transcription factor binding, enzyme binding and cytoskeletal protein binding.

We then performed Kyoto Encyclopaedia of Genes and Genomes (KEGG) pathway analysis on each line and sought out pathways shared across HD lines (Fig. 1e). Genes associated with neuroactive ligand-receptor interaction and calcium signalling were both significantly up- and down-regulated across HD astrocytes, consistent with altered cellular signalling established in GO analysis. PI3K-AKT signalling and MAPK signalling were also significantly disrupted in HD astrocytes. Notably, genes linked to p53 signalling indicative of a DNA damage response were up-regulated in 58Q, 69Q and 75Q astrocytes, but surprisingly not in 125Q and 180Q astrocytes (Fig. 1e). Gene set enrichment analysis (GSEA) for hallmark gene sets showed significant up-regulation in enrichment scores of several pro-inflammatory pathways as well as the p53 pathway for 58, 69 and 75Q astrocytes. (Supplementary Fig. 1). In contrast, several inflammatory pathways appeared down-regulated in 125Q and 180Q astrocytes, as well as glycolysis, fatty acid metabolism and cholesterol homeostasis consistent with dysregulated metabolism.

Genes involved in extracellular matrix (ECM) receptor interactions were significantly up- and down-regulated, with aspects of collagen, laminin and integrin pathways disrupted across HD astrocytes (Supplementary Fig. 2a) (Kanehisa and Goto, 2000). Taken together with significant dysregulation of focal adhesion and reduced expression of

a)

Differentially Expressed Genes

	Up-regulated	Down-regulated
58Q	3192	2634
69Q	4502	5053
75Q	3793	3383
125Q	5292	5087
180Q	4084	4485

Shared	Up-regulated	Down-regulated
58, 69 & 75Q	863	874
125 & 180Q	689	919
All lines	20	34

b)

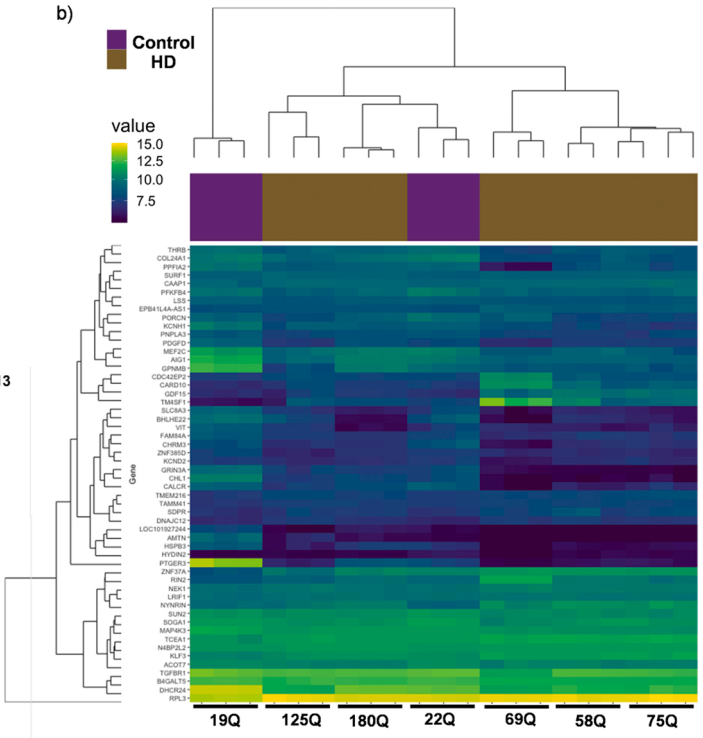

c)

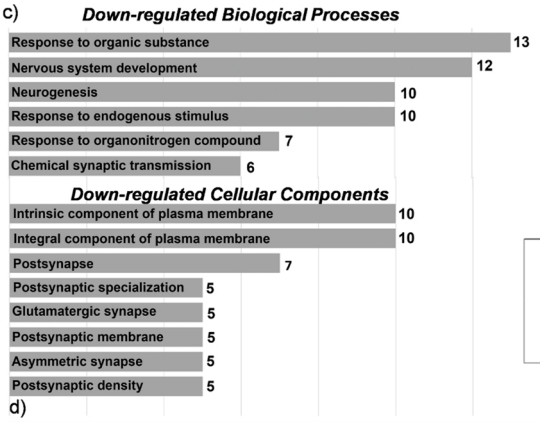

d)

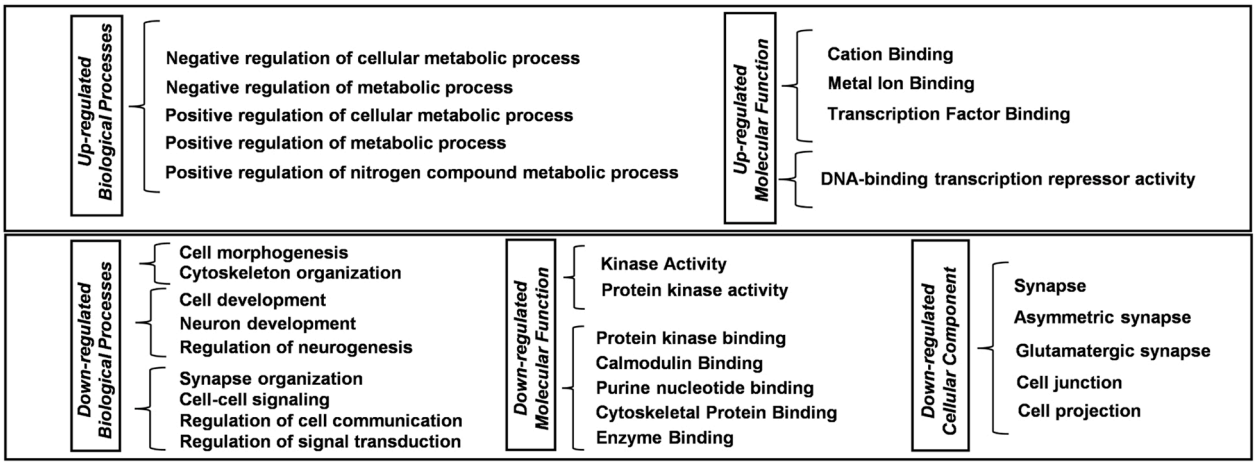

e)

Up-regulated Pathway	58Q	69Q	75Q	125Q	180Q
Neuroactive ligand-receptor interaction					
PI3K-Akt signaling pathway					
MAPK signaling pathway					
Calcium signaling pathway					
ECM-receptor interaction					
Focal adhesion					
Hippo signaling pathway		X			
Rap1 signaling pathway					X
Ras signaling pathway				X	
Cytokine-cytokine receptor interaction			X		
TGF-beta signaling pathway	X	X			
Protein digestion and absorption	X			X	
NF-kappa B signaling pathway			X	X	X
p53 signaling pathway				X	X
Aldosterone-regulated sodium reabsorption	X	X	X		

Down-regulated Pathway	58Q	69Q	75Q	125Q	180Q
Calcium signaling pathway					
Neuroactive ligand-receptor interaction					
PI3K-Akt signaling pathway					
MAPK signaling pathway					
ECM-receptor interaction					
Apelin signaling pathway					
Ras signaling pathway					
Inflammatory mediator regulation of TRP channels					
Focal adhesion					X
Regulation of actin cytoskeleton					X
Phospholipase D signaling pathway				X	X
Cytokine-cytokine receptor interaction		X			
Protein digestion and absorption	X				
TNF signaling pathway	X	X			
Cell adhesion molecules	X	X	X	X	

p<0.001 | p<0.01 | P<0.05 | non-signficant | X Pathway not enriched

(caption on next page)

Fig. 1. IPSC-derived Huntington's Disease astrocytes exhibit transcriptional differences. RNA sequencing was performed on five induced pluripotent stem cell derived HD astrocytes (58Q, 69Q, 75Q, 125Q and 180Q). (a) Differentially expressed genes (DEGS) for each line. Astrocytes with 58–75Q shared a number of DEGs, as did 125–180Q astrocytes, whereas only 24 up-regulated genes and 37 down regulated genes were shared across all HD lines. (b) Heatmap of expression of DEGs shared across all lines. Dendrograms show hierarchical clustering of genes (left) and cell lines (top). Disease state is given for each cell line; 19Q, 22Q =control, HD = Huntington's disease. Individual genes are listed in supplementary table 1b&c (c) Gene Ontology (GO) analysis for all shared, significantly down-regulated genes between HD astrocytes found DEGS to be associated with nervous system development, neurogenesis and synapses. (d) GO analysis of individual lines with shared terms between lines extracted. This highlighted metabolic dysregulation across all HD line as GO terms related to positive and negative regulation of metabolism were signficantly up-regulated. Significantly down-regulated GO terms shared across all lines were linked to neuron development and cell signaling, binding of enzymes and proteins as well as synaptic terms. (e) Kyoto Encyclopedia of Genes and Genomes (KEGG) pathway analysis revealed significant dysregulation of several pathways across HD astrocytes most notably the PI3K-AKT signaling pathway, MAPK signaling pathway and neuroactive ligand receptor interaction suggesting a wide ranging defect in normal astrocyte functions. ECM receptor interactions and Focal adhesion also showed significant dysregulation in HD. $P < 0.001$.

genes associated with cell adhesion molecules in 180Q astrocytes, this suggests that adhesion is altered in HD astrocytes. In IPSC- and ESC-derived astrocytes (45Q, 56Q, 81Q) (Table 1) we found that 48 h after plating, the number of astrocytes attached were significantly lower across all eight HD lines indicative of reduced cell adhesion (Supplementary Fig. 2b). No changes in proliferation were observed that could account for the differences in cell number (Supplementary Fig. 2c).

Weighted correlation network analysis highlighted several modules associated with disease and polyQ length across all HD astrocytes (Supplementary Fig. 3, Supplementary Tables 4 & 5). WGCNA compares expression of genes across multiple samples to define modules, which are clusters of highly interconnected genes, in an unbiased fashion. GO and KEGG analysis of these modules corresponded to data from our GO and KEGG analysis above, including ion channel activity, glutathione metabolism and protein processing (Supplementary Fig. 4).

Further analysis of our WGCNA modules from HD astrocytes revealed significant overlap with modules disrupted in HD patient brain related to HD and polyQ length from two independent cohorts (Hodges et al., 2006; Lin et al., 2016; Neueder and Bates, 2014). Overlap analysis with data from the post-mortem HD patient cortex (Lin et al., 2016), showed significant overlap with the top modules from all HD astrocytes (Fig. 2a). We next separated HD astrocytes into three groups, 58Q–75Q, 125Q and 180Q, based on polyQ length (Supplementary Fig. 5, Supplementary tables 4&5). The top modules from 58Q–75Q astrocytes significantly overlapped with modules from the cortex of the two independent patient cohorts (Fig. 2b,c). These changes grew more pronounced with increasing polyQ length, as in modules from 125Q and 180Q astrocytes we observed significant overlap with modules from the patient cerebellum and caudate in addition to modules from the cortex (Fig. 2d-k). Furthermore, in 125Q and 180Q astrocytes the top WGCNA modules significantly overlapped with top modules from astrocytes obtained from 175Q and R6/2 HD mouse models (Supplementary Figs. 6,7) (Diaz-Castro et al., 2019).

In summary, the most disrupted modules in our HD astrocytes significantly overlapped with the most disrupted modules from HD patient caudate and cortex.

3.2. HD astrocytes exhibit a reactive phenotype and show polyQ length dependent changes in gene expression

Transcriptional data highlighted the significant disruption of pathways involved in inflammation such as MAPK and PI3K/AKT (Fig. 1e), as well as polyQ length dependent changes in inflammatory pathways (Supplementary Fig 1). We thus investigated whether HD astrocytes (45Q, 56Q, 58Q, 69Q, 75Q, 81Q, 125Q, 180Q) presented a reactive phenotype as compared to their respective controls. We first examined expression of intermediate filaments GFAP and Vimentin, as well as of the water channel protein aquaporin 4 (AQP4) which is highly expressed in astrocytes, by immunostaining our astrocyte cultures (Fig. 3a). Expression of these markers as well as glutamine synthetase (Supplementary Fig. 8a) confirmed that our IPSC-derived astrocytes had successfully been differentiated. Only a small number of SOX2-positive neural progenitor cells was still present in both control and HD astrocytes (Supplementary Fig. 8b). As expected in most HD PSC-derived models, we did not find evidence of mHTT aggregation (Supplementary Fig. 8c). We found that GFAP was significantly up-regulated across all HD lines (Fig. 3a) indicative of astrocyte reactivity. We found a similar trend for Vimentin, however this was more variable between astrocyte lines (Fig. 3b). Examining combined control and HD astrocyte values shows that HD astrocytes express significantly more Vimentin. Furthermore, we observed significantly increased AQP4 expression in HD astrocytes, with the exception of 81Q astrocytes where some up-regulation was nonetheless apparent (Fig. 3c). Taken together, HD astrocytes express AQP4 more highly than healthy astrocytes. We found no consistent changes in NF-kB protein levels, as cellular expression was either significantly up- or down-regulated in some of the HD astrocytes (Supplementary Fig. 9). Whilst we detected some statistically significant morphological changes in HD astrocytes in both nuclear and cytoplasmic size as well as nucleus to cytoplasm ratio (Supplementary Fig. 10a-c), these were not polyQ length dependent nor dependent on iPSC versus ESC background and appeared variable between lines.

We further examined expression of genes associated with astrocyte reactivity using QPCR and focused on several HD astrocyte lines with a range of polyQ lengths (45Q, 56Q, 75Q, 81Q, 125Q and 180Q) and normalised them to their respective controls. We found significant up-regulation of *NES* (*NESTIN)* and *S100B* in most HD astrocytes lines (Fig. 4a, b). *NES* has been found to be up-regulated both in immature and reactive astrocytes, however concomitant up-regulation of astrocyte marker, *S100B* (S100 calcium-binding protein B), a protein also upregulated in reactive astrocytes (Brozzi et al., 2009; Cerutti and Chadi, 2000), suggests that their increased *NES* expression may be indicative of a reactive rather than immature phenotype. We found no consistent changes in gene expression of astrocyte marker *ALDH1L1* (*Aldehyde Dehydrogenase 1 Family Member L1*) (Supplementary Fig. 11a). Similarly, expression of *IL-1B* (*Interleukin-1B*) and *ADORA2A* (*Adenosine A2a Receptor*) which has previously been highlighted in transcriptomics data, did not yield consistent differences in gene expression (Supplementary Fig. 11b-d). The A2 marker *S100A10* was significantly down-regulated except in one isogenic line (45Q, 81Q) (Fig. 4c). Interestingly we found polyQ dependent changes in expression of *VEGFA (Vascular Endothelial Growth Factor A)*, *C3* (*Complement Component 3*) and *IL-6* (*Interleukin-6*) (Fig. 4d-f). *VEGFA* was significantly down regulated across HD astrocytes, and to a greater extent the longer the polyQ length. *C3* and *IL-6* were significantly up-regulated in 45Q and 56Q astrocytes, but down-regulated in HD astrocytes with $>$ 75Q. This is somewhat surprising as it would have been expected for markers associated with neurotoxicity to be more highly expressed in HD astrocytes with longer polyQ lengths. It is conceivable that this reflects an impaired inflammatory response in these HD astrocytes, consistent with the GSEA Hallmark enrichment data (Supplementary Fig. 2). Taken together our data supports the idea that HD astrocytes do not exhibit a clear A1 versus A2 response, but do acquire a reactive phenotype. Most notably we provide novel evidence that HD astrocytes show polyQ dependent changes in gene expression.

3.3. PolyQ length-dependent metabolic disruption in HD astrocytes

Astrocyte reactivity in diseases is often accompanied by changes in

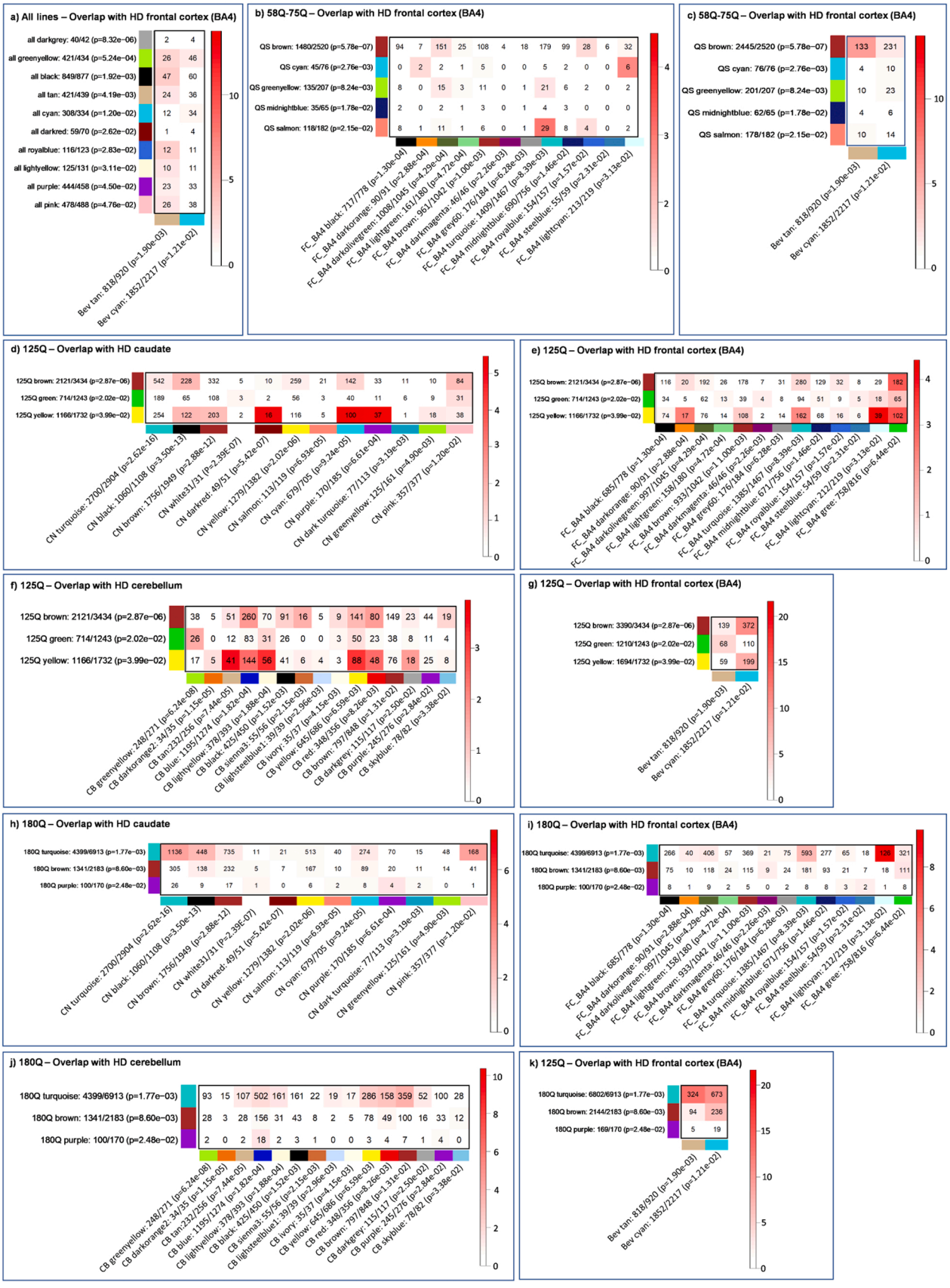

(caption on next page)

Fig. 2. Significant overlap of weighted correlation network analysis (WGCNA) modules from HD astrocytes with post-mortem HD brain samples. Overlap analysis of significantly enriched WGCNA modules was performed between HD astrocytes and HD post-mortem transcriptomic data. HD astrocyte WGCNA modules are given on the y-axis and HD brain modules on the x-axis, each with their significance for HD association. Only modules which reached significance threshold using Fisher's exact test in both dataset are shown. For each module pair the gene count intersection is given, and significance as -log10(p) is indicated by colour, according to the legend. a) Overlap of HD astrocytes (all lines) and HD patient BA4 frontal cortex modules (Lin et al., 2016). b) Overlap of 58Q, 69Q and 75Q HD astrocyte WGCNA modules and HD patient BA4 frontal cortex modules (Neueder and Bates, 2014) c) Overlap of 58Q, 69Q and 75Q HD astrocyte WGCNA modules and HD patient BA4 frontal cortex modules (Lin et al., 2016). d-f) Overlap of HD 125Q astrocyte and HD patient caudate, BA4 frontal cortex and cerebellum modules (Neueder and Bates, 2014). g) Overlap of HD 125Q astrocyte and HD patient BA4 frontal cortex modules (Lin et al., 2016). h-j) Overlap of HD 180Q astrocyte and HD patient caudate, BA4 frontal cortex and cerebellum modules (Neueder and Bates, 2014). k) Overlap of HD 180Q astrocyte and HD patient BA4 frontal cortex (Lin et al., 2016) modules.

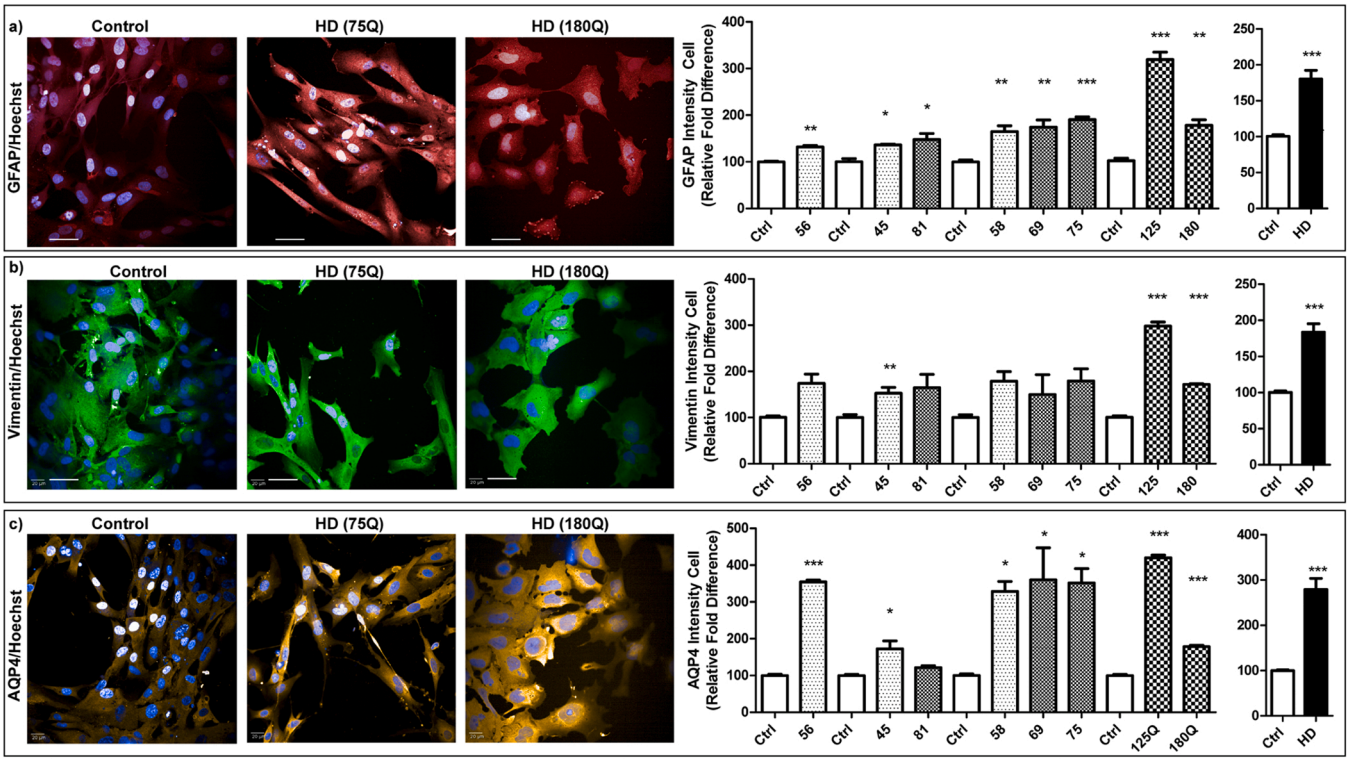

Fig. 3. Huntington's disease (HD) PSC-derived astrocytes exhibit evidence of astrocyte reactivity. Control and HD astrocytes were stained with intermediate filament markers GFAP and Vimentin, as well as Aquaporin 4 (AQP4). Scale bar = 50 μM. (a) GFAP was significantly up-regulated across all HD lines, suggestive of astrocyte reactivity. (b) A trend towards increased Vimentin expression was apparent across all HD lines, however with higher variability than GFAP. (c) Aquaporin 4 expression was significantly up-regulated across the majority of HD astrocytes. * : $p < 0.05$, * *: $p < 0.01$, * ** : $p < 0.001$. Data are presented as mean ± SEM of three astrocyte differentiations of each line, technical replicates n = 6, analyses between each isogenic pair/group was performed by student's t-test or one way ANOVA with Bonferroni correction where appropriate.

astrocyte metabolism, and GO analysis showed that several terms associate with positive and negative regulation of metabolism were significantly up-regulated in our IPSC-derived HD astrocytes (Supplementary Table 3). We carried out metabolic enrichment analysis (MAREA) of RNA sequencing data for 58Q, 69Q, 75Q, 125Q and 180Q astrocytes (Supplementary Figs. 12, 13). Various pathways showed dysregulation in HD astrocytes, common pathways between lines included reduced UREA metabolism in 58, 69, 75 and 125Q astrocytes. MAREA highlighted an up-regulation in key genes involved in fatty acid oxidation in 58–75Q, however a key enzyme (carnitine-acylcarnitine translocase) for long chain fatty acid appeared down-regulated in these astrocytes. Whilst fatty acid oxidation was up-regulated in 125Q astrocytes, it was decreased in 180Q astrocytes with no changes in carnetine-acylcarnitine translocase, which may potentially reflect differences in processing of long chain fatty acids in HD astrocytes. Water metabolism was increased in 69 and 75Q astrocytes only, and citrulline metabolism was down-regulated in 125Q and 180Q astrocytes. Although MAREA clearly indicated metabolic dysregulation in HD astrocytes, it was difficult to draw definite conclusions from these transcriptional changes about the impact on cell behaviour and the pathways mainly affected. Therefore, we carried out biochemical assays to further investigate metabolic defects. As previous research indicates reduced ability of HD astrocytes to take up glutamate, we assessed glutamate uptake in our human astrocytes. As shown in Fig. 5a and Supplementary Fig. 13a, glutamate levels were significantly higher in the culture medium of HD astrocytes than controls regardless of polyQ length. We then examined glucose metabolism in a representative number of astrocyte lines (58, 69, 75, 125 and 180Q) using mass spectrometry and found significantly lower rates of glucose oxidation in 125 and 180Q astrocytes only, consistent with the Hallmark enrichment data (Fig. 5b, Supplementary Fig. 2, 17b). To investigate metabolic changes further, we used the MTT assay which is widely used to assess to measure cellular metabolic activity. MTT is taken up through endocytosis and is reduced by mitochondrial enzymes, endosomal and lysosomal compartments to form MTT formazans (Lü et al., 2012). To account for changes in cell survival, we normalised the assay to cell number using Hoechst. We found significantly up-regulated metabolic activity in HD astrocytes carrying 45–81Q consistent with increased metabolic activity in reactive astrocytes, but down-regulated in 125Q and 180Q astrocytes (Fig. 5c). We next investigated ATP content in HD astrocytes, which showed a trend

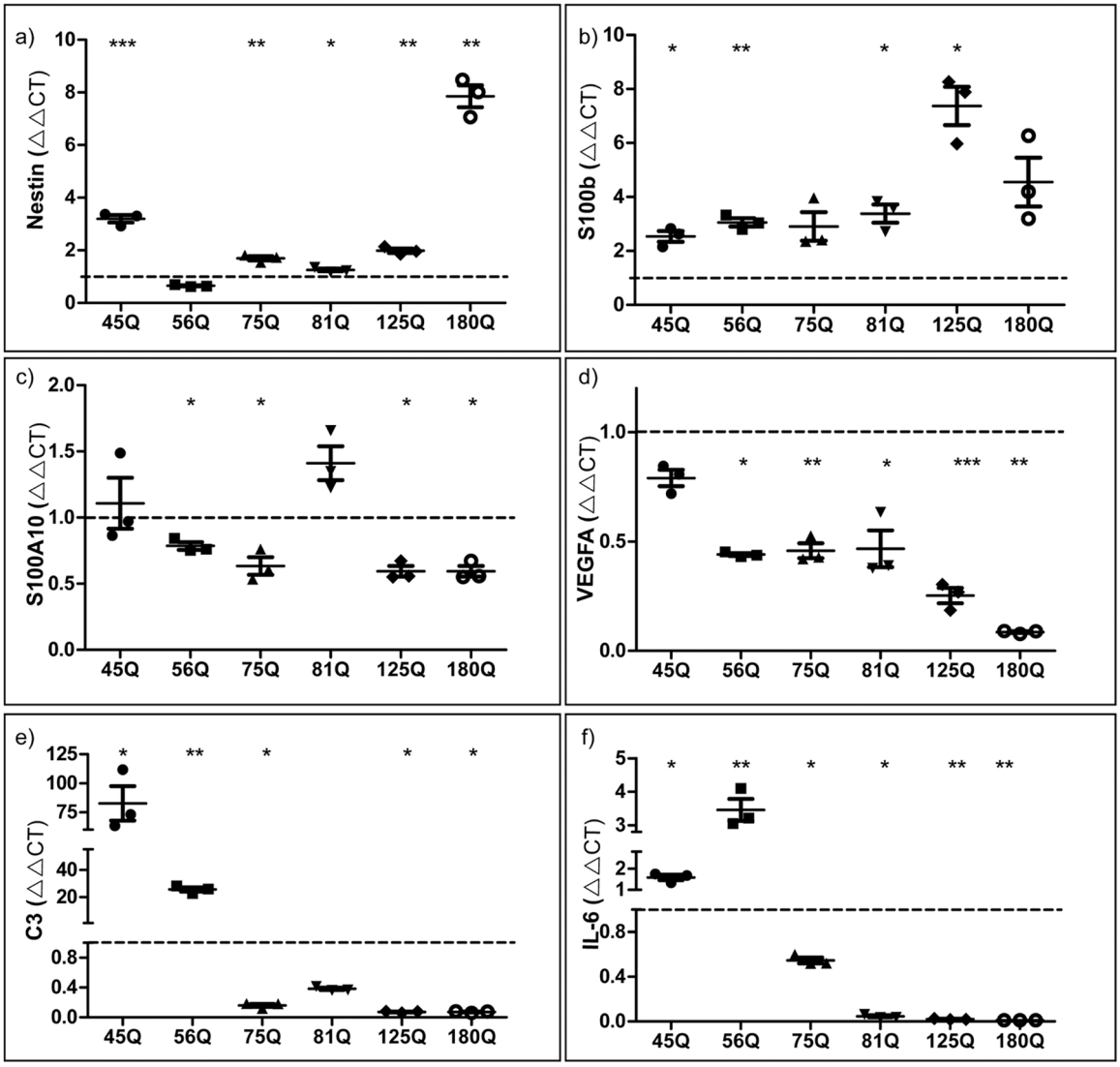

Fig. 4. Huntington's disease (HD) astrocytes exhibit polyQ-length dependent changes in genes associated with astrocyte reactivity. QPCR was performed in biological and technical triplicates and each gene was normalised to three housekeeping genes, *UBC*, *ATP5B* and *EIF4A2* using the delta delta (Δ Δ) CT method. Values were the normalised to their respective control line. (a) Intermediate filament *NES (NESTIN)* was significantly up-regulated across most HD astrocytes compared to respective controls. (b) Astrocyte marker *S100B* was significantly up-regulated across most HD astrocytes, or a noticeable trend could be observed. (c) *S100A10* was significantly down-regulated in 56Q, 75Q,125Q and 180Q astrocytes, however no significant changes are detected in 45Q and 81Q astrocytes. (d) *VEGFA* was significantly down-regulated across HD astrocytes, with greater down-regulation in longer polyQ lengths. (e) *C3* was significantly up-regulated in shorter polyQ length (45&56Q) astrocytes but down-regulated in astrocytes with more than 75Q. (f) *Interleukin-6* (*IL-6*) gene expression was significantly increased in 45&56Q astrocytes, but significantly down-regulated in all other HD astrocytes. * : $p < 0.05$, * *: $p < 0.01$, * ** : $p < 0.001$. Data are presented as mean ± SEM of three astrocyte differentiations of each line, technical replicates n = 3, analyses between each isogenic pair/group was performed by student's t-test or one way ANOVA with Bonferroni correction where appropriate.

towards increased release in 45Q–58Q astrocytes, but was significantly reduced in 69Q-180Q astrocytes (Fig. 5d). Interestingly, we did not observe significant changes in the oxygen consumption of mitochondria used for ATP production (Supplementary Fig. 15), nor did we detect altered gene expression of *SDHA* which is involved in mitochondria complex II, in HD astrocytes (Supplementary Fig. 11c). However, it revealed a significant decrease in spare capacity in 75Q and 180Q astrocytes (Supplementary Fig. 15). This reduction was not observed in 56Q and 125Q astrocytes, suggesting that mitochondrial defects are line specific and not major contributors to early astrocyte dysfunction. We next assessed secretion of lactate and cholesterol, as astrocytes supply both to neurons as metabolic substrates (Fig. 5e,f, Supplementary Fig. 14c,d). Lactate and cholesterol secretion was significantly increased in 45Q–58Q astrocytes, unaffected in 69–81Q astrocytes and significantly down-regulated in 125Q and 180Q astrocytes.

3.4. HD astrocytes exhibit CAG repeat expansion and increased mismatch repair response

Somatic expansion of polyQ length has been linked with earlier HD onset, which we investigated in human HD astrocytes by aging them for 80 days. We detected increases in polyQ length to a minor but significant degree in 58Q astrocytes and to a greater degree in 125 and 180Q astrocytes (Fig. 6a,b). This was accompanied by an increased DNA damage mismatch repair response (MMR) in HD astrocytes. We first assessed gene expression using qPCR and found *HTT* expression to be up-regulated across HD astrocytes consistent with the existing literature (Carter et al., 2014) (Fig. 7a). FAN1 up-regulation has been shown to be protective against CAG expansion in U20S cells (Goold et al., 2019). We did not observe a consistent phenotype across our HD astrocytes, but found significant up-regulation of *FAN1* in 45Q, 75Q and 180Q

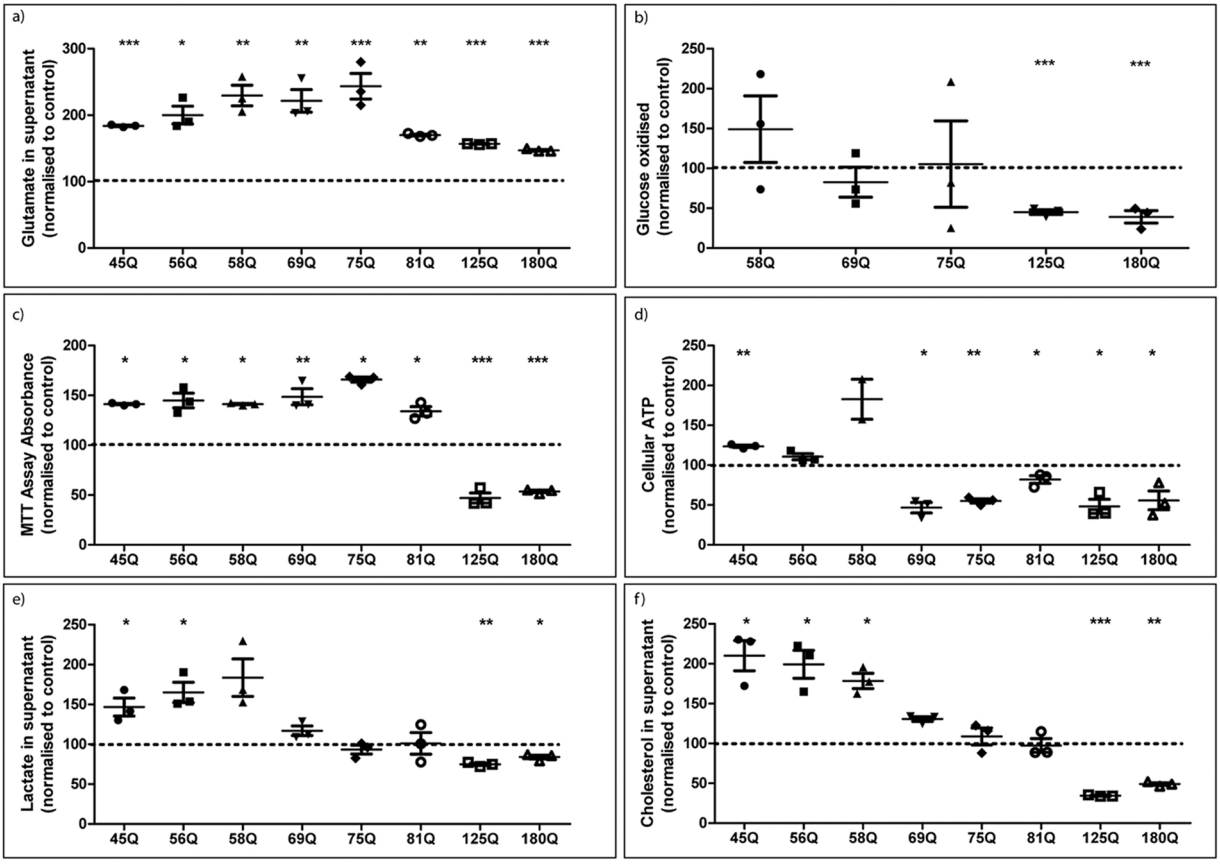

Fig. 5. Huntington's disease (HD) astrocytes exhibit polyQ-length dependent metabolic alterations. All metabolic assays in a,c,d,e and f were normalised to Hoechst counts in a matching duplicate plate. Values were normalised to the respective controls. (a) Glutamate uptake was measured in astrocyte cultures after adding 50 μM Glutamate for half an hour. Glutamate remaining in the supernatant was significantly high in HD astrocytes, suggesting impaired glutamate uptake. (b) Glucose oxidation after 24 h in representative HD astrocytes shows significantly lower rates of glucose metabolism in 125Q and 180Q astrocytes only. (c) Overall metabolic activity was measured by MTT assay. Metabolic activity was significantly increased in HD astrocytes with 45–81Q but significantly decreased in astrocytes with more than 125 Q. (d) ATP secretion was significantly increased in 45Q and unaffected in 56&58Q astrocytes, but significantly down-regulated in astrocytes with more than 69 Q. (e) Lactate secretion was up-regulated in 45–58Q astrocytes, unaffected in 69–81Q astrocytes and significantly down-regulated in 125&180Q astrocytes. (f) Total cholesterol secretion was significantly up-regulated in 45–58Q astrocytes, unaffected in 69–81Q astrocytes and significantly decreased in 125&180Q astrocytes. * : $p < 0.05$, * *: $p < 0.01$, * ** : $p < 0.001$. Data are presented as mean ± SEM of three astrocyte differentiations of each line, technical replicates n = 6, analyses between each isogenic pair/group was performed by student's t-test or one way ANOVA with Bonferroni correction where appropriate.

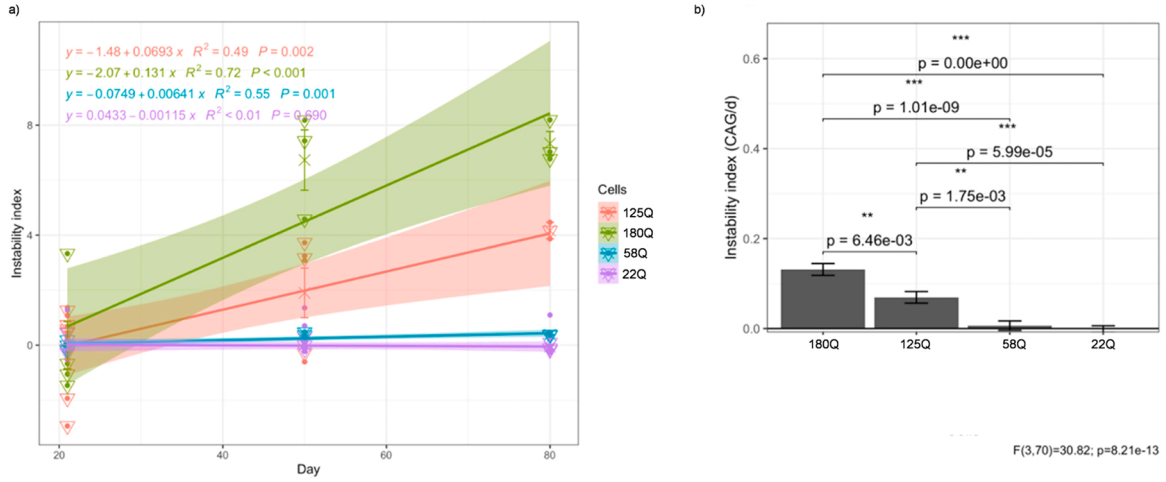

Fig. 6. HD astrocytes exhibit somatic expansion over time. (a) Change in instability index over time for each cell line (Goold et al., 2019). Points represent a distinct differentiation, triangles the average of each differentiation and x's are mean for each timepoint. Linear models are fitted, with the 95 % confidence interval indicated by the shaded region and the equation and p-value for change over time given in the top left. (b) Bar plots of CAG expansion rate, with error bars indicating the standard error. Expansion rates are compared by ANOVA of a linear mixed effects model, with biological replicate as a random effects variable. ANOVA for the effect of cell line on CAG expansion rate is given in the bottom right.

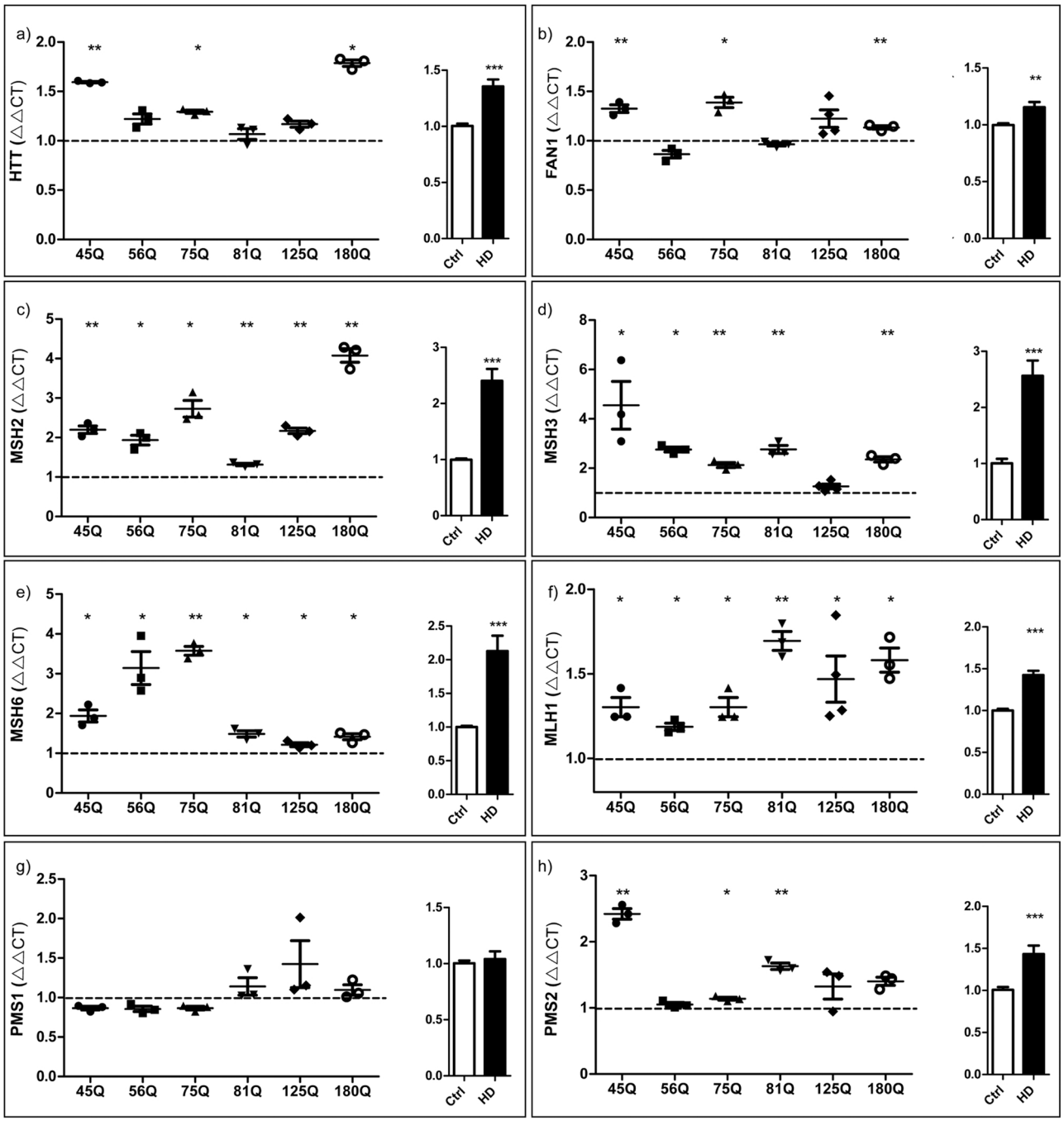

Fig. 7. DNA mismatch repair gene expression in increased in Huntington's Disease (HD) astrocytes. DNA mismatch repair gene expression in increased in Huntington's Disease (HD) astrocytes QPCR was performed in biological and technical triplicates and each gene was normalised to three housekeeping genes, *UBC*, *ATP5B* and *EIF4A2*. (a) *Huntingtin* (*HTT*) gene expression tended to be increased in HD astrocytes, with significant up-regulation in 45Q, 75Q and 180Q astrocytes. (b) *FAN1* was up-regulated in 45Q, 75Q and 180Q astrocytes (c) *MSH2* expression was significantly up-regulated across HD astrocytes. (d) *MSH3* was significantly up-regulated in the majority of HD astrocytes. (e) *MSH6* expression was significantly up-regulated across all HD astrocytes. (f) *MLH1* expression was significantly up-regulated across all HD astrocytes. (g) *PMS1* expression was not significantly altered in HD astrocytes. (h) *PMS2* trended towards increased expression with significantly increased expression in 45Q, 75Q and 81Q astrocytes. * : $p < 0.05$, * *: $p < 0.01$. Data are presented as mean ± SEM of three astrocyte differentiations of each line, technical replicates n = 3, analyses between each isogenic pair/group was performed by student's t-test or one way ANOVA with Bonferroni correction where appropriate.

astrocytes and when samples were pooled in control as compared to HD astrocytes (Fig. 7b). *MSH2*, *MSH3, MSH6* and *MLH1* were significantly up-regulated across all HD astrocytes, suggesting a significant activation of the MMR complex (Fig. 7c-f). We did not observe significant changes in *PMS1*, a member of the DNA mismatch repair mutL/hexB family, though expression appeared down-regulated in 45Q, 56Q and 75Q astrocytes, but was slightly up-regulated in 81Q, 125Q and 180Q (Fig. 7 g). *PMS2* appeared up-regulated across HD astrocytes, with significant up-regulation in 45Q, 75Q and 81Q astrocytes (Fig. 7 h).

We next investigated whether changes in gene expression translated to protein expression (Fig. 8a). We found PMS1 and 2 protein expression to be extremely low and not quantifiable (not shown). FAN1 expression was variable, but trended towards increased expression across HD astrocytes (Fig. 8b). MSH2 expression was significantly up-regulated

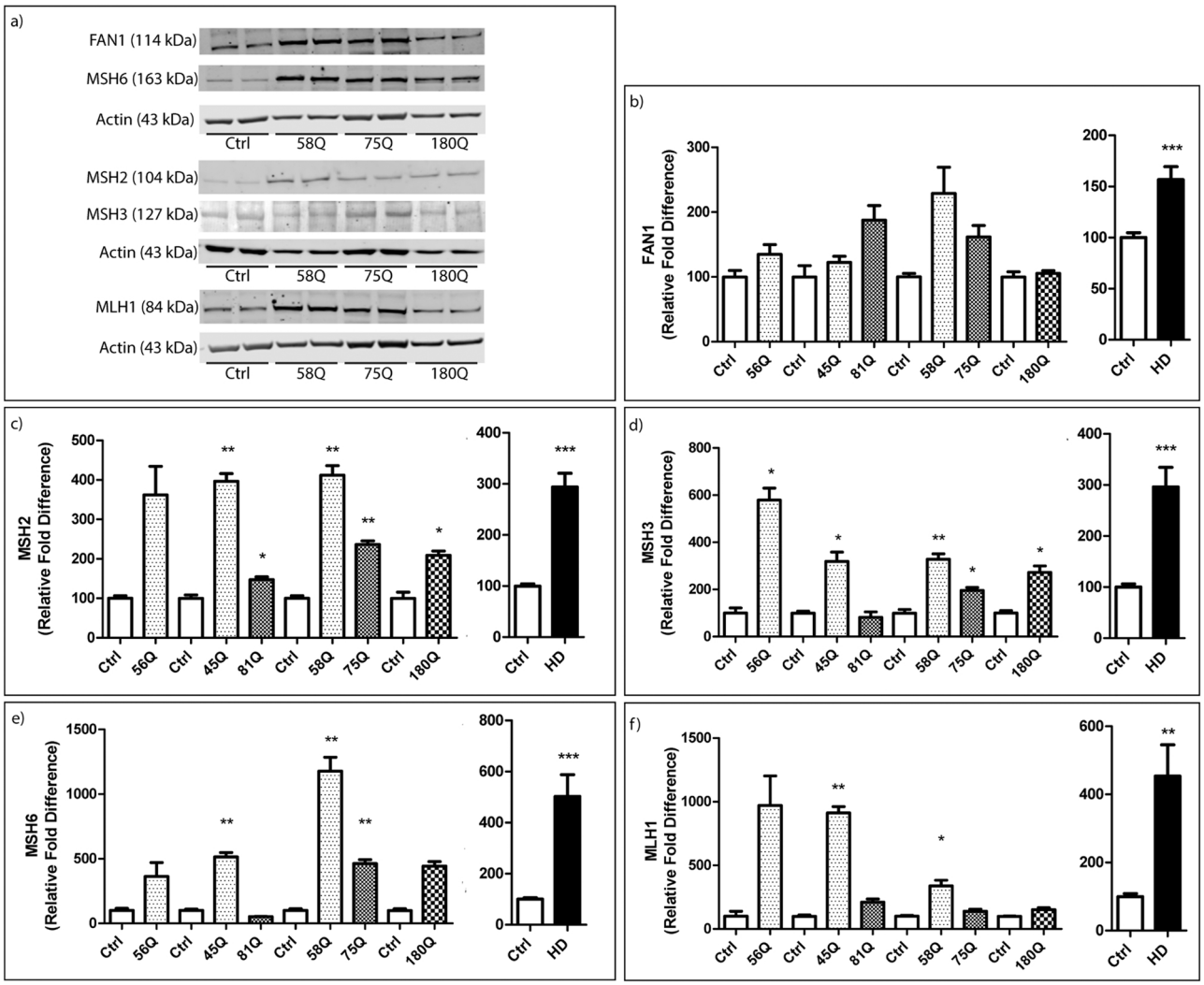

Fig. 8. DNA mismatch repair protein expression is altered in Huntington's Disease (HD) astrocytes. (a) Representative western blots of HD astrocytes (Control, 58Q, 75Q, 180Q) for FAN1, MSH6, MSH2, MSH3 and MLH1. (b) FAN1 expression was variable, with no significant changes detected in individual HD astrocytes lines, but significant up-regulation when data were pooled. (c) MSH2 expression was significantly increased in the majority of HD astrocytes. (d) MSH3 expression was significantly increased in HD astrocytes, with the exception of 81Q astrocytes. (e) MSH6 expression was significantly increased in HD astrocytes, except 56Q and 81Q astrocytes. (f) MLH1 expression was increased in 56Q astrocytes, significantly increased in 45 & 58Q astrocytes, trended towards increase in 75, 81 and 180Q astrocytes. * : $p < 0.05$, * *: $p < 0.01$. Data are presented as mean ± SEM of three astrocyte differentiations of each line, technical replicates n = 3, analyses between each isogenic pair/group was performed by student's t-test or one way ANOVA with Bonferroni correction where appropriate.

across HD astrocytes with the exception of 56Q astrocytes (Fig. 8c). Similarly MSH3 expression was significantly up-regulated across HD astrocytes, except in 81Q astrocytes, as was MSH6 expression with the exception of 81Q and 180Q astrocytes (Fig. 8d,e). MLH1 trended towards increased expression but was only significantly increased in 45Q and 58Q astrocytes (Fig. 8 f). Pooling control and HD astrocytes reveals a significant up-regulation of both FAN1 and MMR proteins, though the increase in MMR protein expression is greater than that of FAN1.

3.5. HD astrocytes exhibit increased cell death, oxidative DNA damage and double strand breaks

Our transcriptomics data highlighted several pathways that could potentially be involved in cell death and DNA damage, including PI3K/AKT signalling, MAPK signalling and p53 signalling (Fig. 1d). Furthermore, Hallmark analysis highlighted up-regulation of genes involved in DNA repair in several lines (Supplementary Fig. 1).

We examined cell death in astrocytes using propidium iodide to label dead cells (Fig. 9a), and found a significant increase in dead cell percentage in all HD astrocytes as compared to controls (Fig. 9b). To assess oxidative damage, astrocytes were stained for 8OHdG, as well as yH2AX and 53BP1 which are recruited to double strand breaks (Fig. 9c). Expression of 8OHdG was significantly increased in HD astrocytes, with the exception of 81Q and 58Q astrocytes where a trend towards up-regulation was apparent (Fig. 9d). Nuclear Intensity of yH2AX and 53BP1 was also significantly increased across HD astrocytes, indicative of increased DNA double strand breaks (Fig. 9e,f). This appeared particularly pronounced in 125Q and 180Q astrocytes (Supplementary Fig. 16). Changes in yH2AX and 53BP1 protein expression detected by western blots were consistent with the immunostaining data, confirming that HD astrocytes carry a large DNA damage burden (Fig. 9 g).

We next investigated the DNA damage response of HD astrocytes by assessing expression of relevant proteins encoded by genes identified as differentially expressed in our RNA seq analysis (Fig. 10a). We first assessed expression of NIMA related Kinase 1 (NEK1), thought to be involved in the early DNA damage response, as RNA seq data for 58Q, 69Q, 75Q and 125Q astrocytes showed *NEK1* up-regulation (Fig. 1b, Supplementary Table 1). However, with the exception of 56Q astrocytes, NEK1 protein expression in HD astrocytes either trended towards decrease (45Q, 58Q) or was significantly lower (75Q, 81Q and 180Q) in

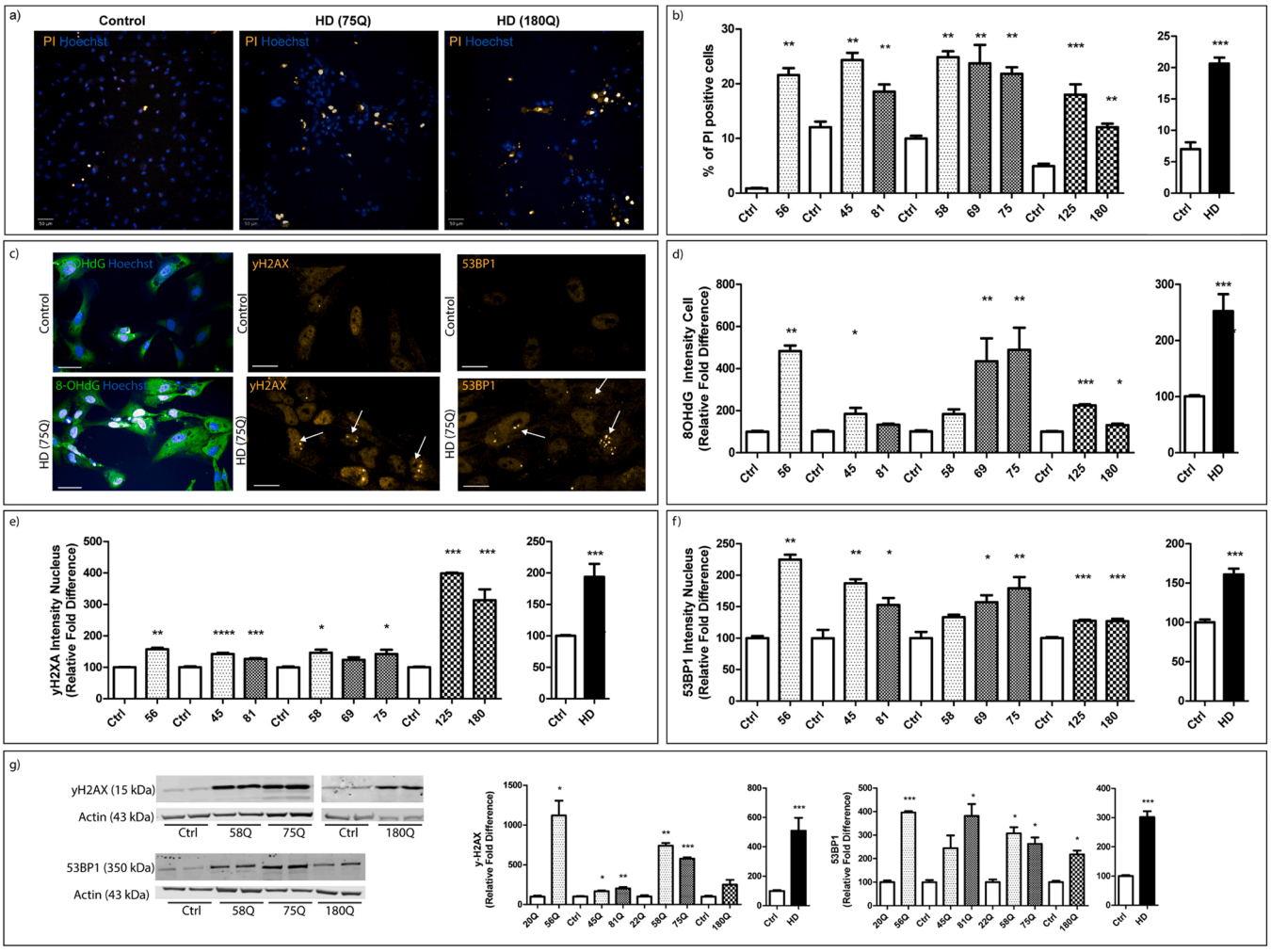

Fig. 9. Huntington's disease (HD) astrocytes exhibit increased cell death and DNA damage. (a) Astrocytes were stained with Propidium Iodide (PI) to stain dead cells and counterstained with Hoechst to label all nuclei. Scale bar = 50 μM. (b) PI/Hoechst staining revealed significantly higher level of cell death in HD astrocytes. (c) Astrocytes were stained with 8-OHdG to stain for oxidative DNA damage, yH2AX and 53BP1 to label DNA double strand breaks. Nuclei were counterstained with Hoechst. Arrows indicate double strand break foci. Scale bar = 20 μM. (d) 8-OHdG intensity was significantly increased in 56Q, 45Q< 69Q, 75Q, 125Q and 180Q astrocytes, with a trend towards increase in the remaining lines. Pooling control and HD astrocytes found significantly higher expression of 8-OHdG. (e) yH2AX staining was quantified by measuring staining intensity in all nuclei, which was significantly higher across most HD astrocytes. (f) Nuclear intensity of 53BP1 was significantly higher across HD astrocytes than their respective controls. (g) Western blotting for yH2AX and 53BP1 revealed significantly higher expression across HD astrocytes indicative of increased DNA damage. * : $p < 0.05$, * *: $p < 0.01$, * ** : $p < 0.001$. Data are presented as mean ± SEM of three astrocyte differentiations of each line, technical replicates n = 3, analyses between each isogenic pair/group was performed by student's t-test or one way ANOVA with Bonferroni correction where appropriate.

a polyQ dependent manner (Fig. 10b). When we excluded 56Q astrocytes as an outlier as the values where 2.8 times higher than the standard deviation, and pooled values from HD astrocytes, we found a significant decrease in HD versus control.

We then investigated expression of p53, as *TP53* was the most up-regulated gene in our RNA seq data for 58Q, 69Q and 75Q astrocytes, but unchanged in 125Q astrocytes and decreased in 180Q astrocytes (Supplementary table 1). Protein expression of p53 mirrored RNA expression, with significant up-regulation in HD astrocytes, apart from 180Q astrocytes, where expression trended towards decrease (Fig. 10c). Next, we assessed expression of RAD51, which contains a p53 binding element and is essential for homologous recombination in response to DNA damage. RAD51 was up-regulated or unchanged in 45Q–58Q astrocytes, trended towards decrease in 75Q and 81Q astrocytes and is significantly decreased in 180Q astrocytes in a polyQ length dependent manner (Fig. 10d).

ATM expression was significantly increased in HD astrocytes or trended towards increase (75Q, 180Q) Fig. 10e,f). Phosphorylated (p)-ATM was barely detectable in our astrocyte cultures (not shown) and hence was not quantified. Finally, AKT and p-AKT expression were assessed. AKT showed variable levels of expression across HD lines, but trended towards increased expression whereas up-regulation of p-AKT was more pronounced (Supplementary Fig. 17a,b). We found this also to be the case for the p-AKT/AKT ratio (Fig. 10 g). Pooling of HD astrocyte lines showed a significant increase of ATM, AKT p-AKT and p-AKT/AKT ratio expression in HD astrocytes versus controls, consistent with an increased DNA damage response. Together, these data suggest that the increased and sustained DNA damage contributes to astrocyte dysfunction in HD.

Finally, we compared variability within our control lines (Supplementary Figs. 18, 19) for both immunostaining and qPCR data. We found that our iPSC-derived astrocytes clustered together, as did the ESC-derived astrocytes, and differences were largely found between iPSC derived control astrocytes and ESC-derived astrocytes. These could be due to reprogramming techniques, or iPSC vs ESC genetic background. However, this strengthens our approach of largely using

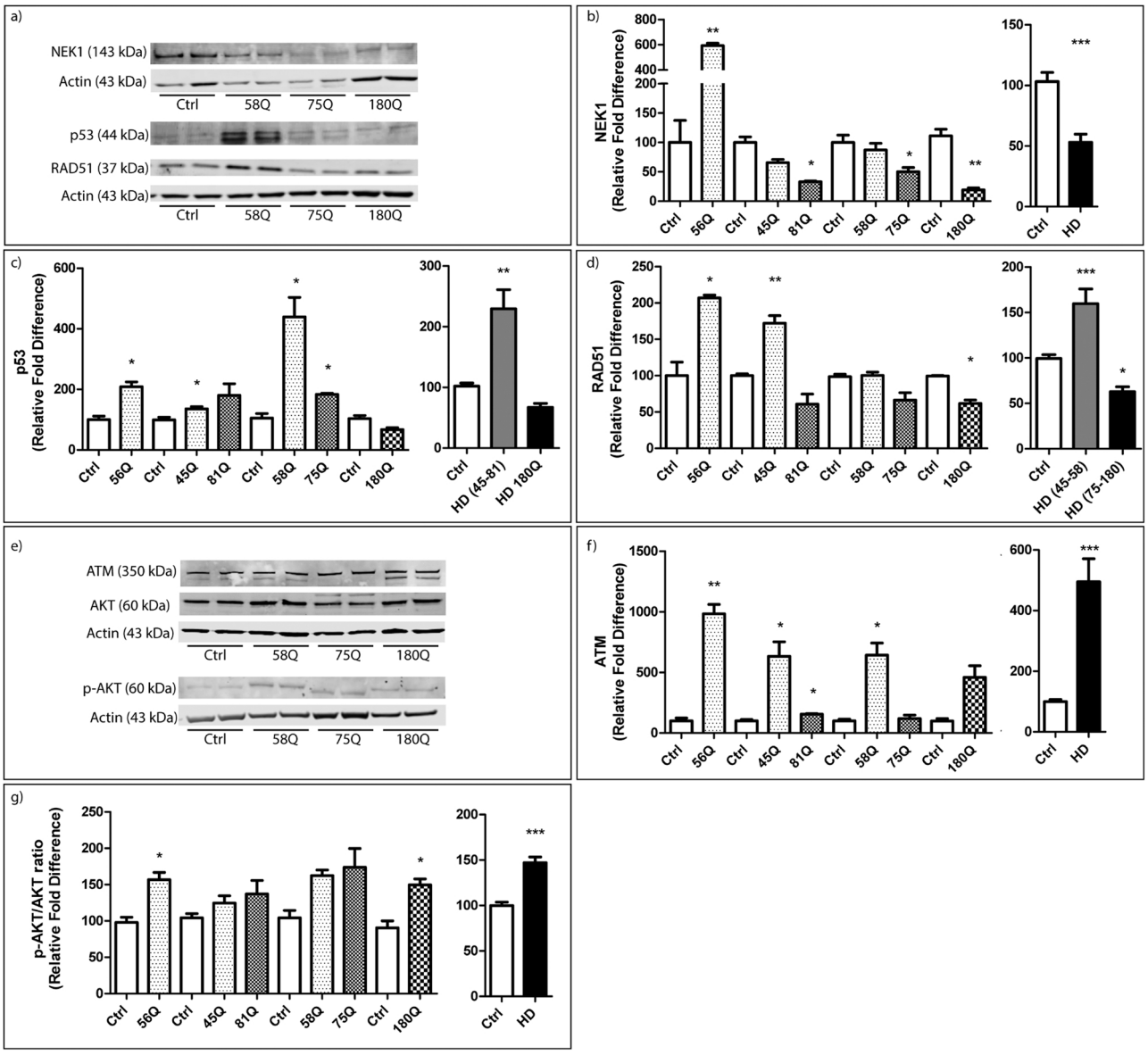

Fig. 10. Huntington's disease (HD) astrocytes exhibit significant dysregulation of the DNA damage response. (a) Representative western blots of HD astrocytes (Control, 58Q, 75Q, 180Q) for NEK1, p53, RAD51, normalised to Actin. (b) NEK1 expression was significantly increased in 56Q astrocytes, unaffected in 45 & 58Q astrocytes and significantly lower in 75,81 & 180Q astrocytes. Pooling HD astrocyte data and excluding 56Q astrocytes shows significant down-regulation of NEK1. (c) p53 expression was significantly higher in 45–75Q astrocytes, with 81Q astrocytes trending towards higher expression. In contrast 180Q astrocytes trended towards lower p53 expression. (d) RAD51 expression was significantly increased in 45 and 56Q astrocytes, unaffected in 58 – 81Q astrocytes and significantly decreased in 180Q astrocytes. (e) Representative western blots of HD astrocytes (Control, 58Q, 75Q, 180Q) for ATM, AKT and phosphorylated(p)-AKT normalised to Actin. (f) ATM expression was significantly increased across the majority of HD astrocytes, with the exception of 75Q and 180Q astrocytes which trended towards increased expression. (e) The p-AKT to AKT ratio was variable across HD astrocytes, with only 56Q and 180Q astrocytes showing a significant up-regulation compared to their respective control. * : $p < 0.05$, * *: $p < 0.01$, * ** : $p < 0.001$. Data are presented as mean ± SEM of three astrocyte differentiations of each line, technical replicates n = 3, analyses between each isogenic pair/group was performed by student's t-test or one way ANOVA with Bonferroni correction where appropriate.

isogenic lines and using iPSC derived controls as comparisons for iPSC derived 125Q and 180Q astrocytes.

4. Discussion

Here we have reported significant transcriptional changes in human PSC-derived HD astrocytes, as well as polyQ dependent phenotypes in astrocyte reactivity and metabolism. We show that human HD astrocytes carry a large DNA damage burden, DNA repair pathway activation and somatic expansion, providing a molecular framework to recent findings suggesting contribution of DNA damage response pathways to disease progression.

4.1. HD astrocytes display extensive transcriptional changes

Bulk RNA sequencing revealed widespread transcriptional dysregulation in IPSC-derived HD astrocytes, with large overlap of dysregulated genes in lines with similar polyQ lengths. Notably, despite a large range of polyQ lengths, we found significantly up-and down-regulated genes that were shared across all HD astrocytes. Dysregulation across several crucial pathways could have widespread consequences on astrocyte function, such as that of MAPK and PI3K/AKT pathways which are

associated with apoptosis, inflammation and DNA damage in HD astrocytes (Kaminska et al., 2009; Karimian et al., 2019; Lee et al., 2006; Rezatabar et al., 2019; Xie et al., 2004). Changes in their expression are likely to have extensive consequences including the ability of HD astrocytes to perform crucial tasks such as help maintain neuronal homeostasis. GO analysis highlighted that genes associated with cell signalling were highly disrupted, consistent with what has been observed in mouse models and IPSC models (Garcia et al., 2019; Jiang et al., 2016). Furthermore, ECM receptor interaction, and focal adhesion molecules have a major impact on synaptic behaviour (Hillen et al., 2018; Kerrisk et al., 2014), suggesting a widespread disruption of astrocytic cell signalling in our cultures as an early phenotype. Dysregulation of cell adhesion molecules has been reported in HD post-mortem brains but it has not been previously shown to occur in HD astrocytes specifically (Ratovitski et al., 2016). Alongside endothelial cells, astrocytes are crucial in maintaining blood brain barrier integrity and cell adhesion molecules mediate these interactions (Abbott et al., 2006; Hawkins and Davis, 2005). Reduced adhesion of our HD astrocytes in culture confirms that disruption of these pathways has significant consequences on HD astrocytes, which may result in altered blood brain barrier function in HD.

Importantly, we found novel evidence that a significant number of WGCNA modules associated with disease and polyQ length in human HD astrocytes overlapped with WGCNA modules from two independent HD post mortem cohorts (Lin et al., 2016; Neueder and Bates, 2014). This was most pronounced for the cortex and caudate, the most affected regions of the HD brain, suggesting a significant contribution of astrocytes to HD disease progression. Notably, overlap increased with increasing polyQ length in our HD astrocytes, possibly indicating that phenotypes in 125 and 180Q reflect astrocyte biology in the end stage of the disease. Overlap with mouse data (Diaz-Castro et al., 2019) was only significant in 125Q and 180Q astrocytes, increasing with age of mice. This suggests that mouse models may not capture the range of phenotypes observed in lower polyQ lengths and further highlights the importance of using models that can allow one to investigate shorter polyQ lengths.

4.2. *Changes in gene expression and metabolism in HD astrocytes are polyQ length-dependent*

Our data highlights evidence of astrocyte reactivity, including upregulation of GFAP and Vimentin, as well as AQP4 which has been shown to be upregulated in reactive astrocytes (Ikeshima-Kataoka, 2016). Astrocyte reactivity and activation of pro-inflammatory pathways have been reported in HD astrocytes (Haim et al., 2015; Hsiao et al., 2013; Khakh et al., 2017; Rueb et al., 2015). Whether HD astrocytes can be clearly assigned to A1 or A2 (neurotoxic versus neuroprotective) astrocyte disease states (Escartin et al., 2021; Liddelow and Barres, 2017) remains unclear. Activation of JAK/STAT and NF-kB pathways in neurotoxic astrocytes has been reported in some models, but not others. Bulk RNA seq of mouse models and human post mortem data has indicated substantial heterogeneity in HD astrocytes, and little evidence to support an entirely neurotoxic phenotype (Diaz-Castro et al., 2019). Amongst the genes up-regulated across all HD astrocytes in our RNA seq data was *TM4SF1*, a gene associated with an A2 astrocyte state (Ceyzériat et al., 2018; Neal et al., 2018). Our qPCR data revealed up-regulation of A2 marker *S100A10*, except in the SUES line astrocytes, possibly due to line specific differences. However, when we examined A1 markers *C3*, *IL-6*, as well as *VEGFA*, we found surprising polyQ length dependent differences in gene expression. Whilst *C3* and *IL-6* expression was significantly increased in shorter polyQ-length HD astrocytes (45Q, 56Q), their expression was significantly down-regulated in longer lengths. (Diaz-Castro et al., 2019) suggested that HD astrocytes progressively lose their essential functions, and the phenotypes observed in our cultures may reflect either an accelerated disease progression of longer length astrocytes or an inability to respond to disease states. *C3* expression is commonly associated with negative pro-inflammatory phenotypes in astrocytes, however it may serve essential functions and it has been shown that *C3* knockout may actually accelerate disease progression in Prion disease (Hartmann et al., 2019). *VEGFA* expression was reduced in all HD astrocytes, however expression decreased the longer the polyQ length. VEGFA reduction in HD astrocytes is consistent with reduced VEGF levels observed in peripheral blood mononuclear cells of pre-manifest and manifest HD patients (Cesca et al., 2015). Given that *VEGFA* is associated with a neuroprotective phenotype, it may reflect an inappropriate disease response in our HD astrocytes and further drive astrocyte dysfunction.

Changes in metabolism have been reported in pre-symptomatic and symptomatic HD patients as well as mouse models however it is not clear to which extent this is driven by astrocytes (Boussicault et al., 2014; Mochel and Haller, 2011; Polyzos et al., 2019; Shin et al., 2013). GO analysis highlighted up-regulation of genes linked to GO terms for both positive and negative regulation of metabolism shared across all lines, but also line specific terms. We also found significant disruption of carbon based metabolism using metabolic enrichment analysis; this is consistent with previous identification of several of these metabolites such as urea and citrulline in a sheep model of HD (Skene et al., 2017). Increased fatty acid metabolism as highlighted by MAREA is consistent with a shift to fatty metabolism in the striatum of HD mice (Polyzos et al., 2019). Crucially, when assessing other metabolic activities that are essential to astrocyte function, we found novel intriguing polyQ dependent changes. Up-regulation of metabolic activity and increased release of lactate and cholesterol in 45Q–58Q astrocytes appears in line with increased astrocyte reactivity and matches the increased release of C3 and IL-6 in these astrocytes. Brain hypermetabolism, thought to be a compensatory mechanism, is significantly correlated with disease severity and may negatively affect brain structures (Gaura et al., 2017). Whilst we see some evidence that 69Q–81Q astrocyte show some increased overall metabolic activity, ATP production or turnover is reduced. This could reflect energy depletion in HD astrocytes, which in turn may contribute to astrocyte stress and dysfunction. Notably, all metabolic activity and release of metabolites in 125Q and 180Q astrocytes was reduced. As observed here in 125Q and 180Q astrocytes, glucose metabolism appears to be reduced in the cortex of HD patients (Martin et al., 1992). Reduced cholesterol is commonly reported in human post mortem brains (Kreilaus et al., 2016) and mouse models (Valenza et al., 2010, 2015), which have similar polyQ lengths as our 125Q and 180Q astrocytes. Furthermore, Valenza et al. (2010) found polyQ dependent cholesterol reductions in HD mice, with the most pronounced reduction in mice with the longest polyQ length. Our data indicate for the first time that this decrease is likely driven by altered astrocyte cholesterol metabolism. It is possible that HD astrocytes up-regulate metabolic activity as an early disease response but this decreases as disease burden accumulates and astrocytes are unable to maintain their function and response. This may explain why cholesterol is reduced in postmortem brains with similar polyQ lengths to our 45Q–58Q astrocytes, despite their early increased release of metabolites. Astrocytes produce the majority of brain cholesterol, which is required for normal brain function (Ferris et al., 2017). Similarly, they are also a crucial source of lactate and ATP for neurons (Harada et al., 2016; Mächler et al., 2016; Magistretti and Allaman, 2013; Xiong et al., 2018), and reduced secretion of ATP and lactate have been shown to increase neuronal stress. Altered secretion of metabolites by HD astrocytes could result in impaired neuron homeostasis hence represent one mechanism driving disease progression.

4.3. *HD astrocytes exhibit an increased MMR response and somatic CAG repeat expansion*

The mismatch repair pathway has been linked to somatic expansion of polyQ length, which is associated with earlier disease onset, and we found evidence of significant somatic expansion in HD astrocytes.

MSH2, MSH3 and MLH1 have been shown to promote CAG expansion, whilst FAN1 appears to protect against CAG repeat expansion (Goold et al., 2019, 2021; Maiuri et al., 2019). The majority of MMR pathway genes assessed were up-regulated on both gene and protein level across HD astrocytes regardless of polyQ length. It is thought that in the brain, cell types vulnerable to degeneration in HD exhibit greater somatic expansion, with individuals inheriting a larger number of CAG repeats exhibiting greater somatic expansion. CAG repeat expansion in glia has previously been reported, although at least one study suggested that this was to a lesser extent than in neurons (Claassen and Lahue, 2007; Gonitel et al., 2008; Shelbourne et al., 2007). Given the expression profiles we found, it seems likely the CAG repeat expansion we observe is the result of increased MMR gene expression, rather than reduced FAN1 expression. One possibility is that increased DNA damage activates MMR, during which strand slippage leads to CAG expansion. MMR proteins may also modify disease progression through interaction with other DNA repair factors such as ATM and TP53 (Luo et al., 2004; Peters et al., 2003).

4.4. Increased DNA damage is present in HD astrocytes

Here, for the first time in HD astrocytes, we reported significantly higher expression of yH2Ax and 53BP1, indicating a greater occurrence of DNA double strand breaks (Panier and Boulton, 2014; Podhorecka et al., 2010), as well as increased expression of 8-OHdG indicative of oxidative DNA damage (Valavanidis et al., 2009). Several pathways from the bulk RNA seq analysis hinted at up-regulation of the DNA damage response in HD astrocytes, as well as dysregulation of several pathways potentially involved in DNA damage. Notably, two of the genes up-regulated across all IPSC-derived astrocytes are thought to be involved in the DNA damage response, *NEK1* and *CAAP1/C9orf82*. NEK1 has been linked to the early DNA damage response (Chen et al., 2011b), where it is located downstream of ATM and is involved in cell cycle arrest to facilitate double strand break repairs (Pelegrini et al., 2010). Despite up-regulation at the gene level, NEK1 protein expression was reduced across most HD astrocytes and this may reflect increased turnover or rapid degradation of NEK1. However, it has previously been shown that NEK1 knockdown can result in DNA damage accumulation and impaired DNA damage response (Higelin et al., 2018). NEK1 is also required for the maintenance of genome stability (Chen et al., 2011a). It is conceivable that lower NEK1 levels in HD astrocytes could be an indication of impairments in the DNA repair response.

TP53 plays a prominent role in DNA repair, and mHTT has been show to bind to it and affect its transcription directly (Bae et al., 2005; Feng et al., 2006). Interestingly, gene expression of *TP53* was up-regulated in 58Q–75Q astrocytes, unaffected in 125Q astrocytes and down-regulated in 180Q astrocytes, with the protein data matching this trend. HD astrocytes with greater polyQ lengths seem to display greater impairment in DNA damage response. Indeed, we have found evidence of an unexpected DNA damage response, as RAD51 expression follows a similar pattern as p53. This is of interest, as, while in small cell lung carcinoma lines p53 binding to RAD51 appears to reduce its activation (Arias-Lopez et al., 2006). However, this certainly does not appear to be the case 45Q–58Q astrocytes, where both p53 and RAD51 are up-regulated.

Consistent with previous data from HD mouse models, we observed up-regulation of ATM, AKT and p-AKT (Colin et al., 2005; Maiuri et al., 2017, 2019) as well as an increase in the proportion of p-AKT to AKT in HD astrocytes compared to controls. Whilst these proteins are crucial for the DNA damage response, prolonged activation of ATM has been shown to be toxic to cell survival in HD and may negatively affect astrocytes in the long term. In summary, we find that HD astrocytes carry a large burden of oxidative DNA damage and DNA double strand breaks. Whilst we see evidence for a DNA damage response, we observe disruption in the expression of specific DNA repair response proteins which could lead to further accumulation of DNA damage.

Taken together, our data are consistent with the hypothesis that DNA damage in HD astrocytes contributes to early astrocyte dysfunction and increases vulnerability to cell death and highlight the need to target astrocytes in the development of novel therapies. Therefore, iPSC-derived HD astrocytes could provide a novel model to investigate repeat expansion and DNA damage in HD, as well as possible therapeutic interventions.

5. Conclusion

In conclusion, we find that PSC-derived astrocytes present a valid model of astrocyte biology in HD as they showed significant overlap of transcriptional changes in HD postmortem brains which further suggests that astrocyte play a substantial role in HD pathogenesis. We have provided evidence of novel phenotypes affecting HD astrocytes regardless of polyQ length, such as increased astrocyte reactivity, changes in cell adhesion and most notably DNA damage, as well as an altered DNA damage response. Furthermore, we have provided evidence for the first time that HD astrocytes exhibit polyQ dependent phenotypes in the expression of inflammatory factors and most notably in metabolic activity. Our results highlight the importance of investigating the role of glia in neurodegenerative disease as well as heterogeneity of astrocytic responses in HD.

Author contributions

JL designed and performed the research, analysed the data and drafted the manuscript, **OG** generated the 19Q IPSC control line, optimised, performed and analysed the Seahorse experiments, **MF** performed and analysed somatic expansion experiments, wrote scripts for RNA sequencing analysis, performed WGCNA analysis on the HD astrocyte data set and performed overlap analysis with other HD WGCNA data sets, **HG** contributed to the qPCR experiments and analysis, **SE** performed and analysed the glucose oxidation experiments, SK performed the pilot experiments, **AN** performed WGCNA analysis on the Lin et al. (2016) data set, PF input on the scientific background of the paper and was involved in the compilation of the manuscript, **SJT** led the research and all authors commented on the final version.

Declaration of Competing Interest

The authors declare no competing interests in this work submitted in this paper.

Data availability

All data sets will be made available upon publication.

Acknowledgements

This work was supported by CHDI Foundation. It was also supported by the UK Dementia Research Institute which receives its funding from DRI Ltd, funded by the UK MRC, Alzheimer's Society and Alzheimer's Research UK. It relied on MRC funding to the MRC Dementia Platform UK (MR/M02492X/1) and MRC core funding to the High-Content Biology Platform at the MRC Laboratory for Molecular Cell Biology at UCL (LMCB; MC_U12266B). Further support was received from GOSH BRC funding. We thank Prof Ali Brivanlou and Dr Alessia Deglincerti at the Rockefeller University for reprogramming the HD Family iPSCs, and Prof Mahmoud Pouladi and Dr Kagistia Utami at the Agency for Science, Technology and Research, Singapore, and National University of Singapore for their kind gift of the IsoHD ESCs. The graphical abstract was generated with Biorender.

Appendix A. Supporting information

Supplementary data associated with this article can be found in the

online version at doi:10.1016/j.pneurobio.2023.102448.

References

Abbott, N.J., Rönnbäck, L., Hansson, E., 2006. Astrocyte-endothelial interactions at the blood-brain barrier. Nat. Rev. Neurosci. 7, 41–53.

Andrew, S., Goldberg, P., Kremer, B., Telenius, H., Theilmann, J., Adam, S., Starr, E., Squitieri, F., Lin, B., Kalchman, M., et al., 1993. The relationship between trinucleotide (CAG) repeat length and clinical features of Huntington's disease. Nat. Genet. 4, 221–226.

Arias-Lopez, C., Lazaro-Trueba, I., Kerr, P., Lord, C.J., Dexter, T., Iravani, M., Ashworth, A., Silva, A., 2006. p53 modulates homologous recombination by transcriptional regulation of the RAD51 gene. EMBO Rep. 7, 219–224.

Askeland, G., Dosoudilova, Z., Rodinova, M., Klempir, J., Liskova, I., Kuśnierczyk, A., Bjørås, M., Nesse, G., Klungland, A., Hansikova, H., et al., 2018. Increased nuclear DNA damage precedes mitochondrial dysfunction in peripheral blood mononuclear cells from Huntington's disease patients. Sci. Rep. 8, 1–9.

Bae, B., Il, Xu, H., Igarashi, S., Fujimuro, M., Agrawal, N., Taya, Y., Hayward, S.D., Moran, T.H., Montell, C., Ross, C.A., et al., 2005. p53 mediates cellular dysfunction and behavioral abnormalities in Huntington's disease. Neuron 47, 29–41.

Benraiss, A., Mariani, J.N., Osipovitch, M., Cornwell, A., Windrem, M.S., Villanueva, C. B., Chandler-Militello, D., Goldman, S.A., 2021. Cell-intrinsic glial pathology is conserved across human and murine models of Huntington's disease. Cell Rep. 36, 109308.

Birger, A., Ben-Dor, I., Ottolenghi, M., Turetsky, T., Gil, Y., Sweetat, S., Perez, L., Belzer, V., Casden, N., Steiner, D., et al., 2019. Human iPSC-derived astrocytes from ALS patients with mutated C9ORF72 show increased oxidative stress and neurotoxicity. EBioMedicine 50, 274–289.

Boussicault, L., Hérard, A.S., Calingasan, N., Petit, F., Malgorn, C., Merienne, N., Jan, C., Gaillard, M.C., Lerchundi, R., Barros, L.F., et al., 2014. Impaired brain energy metabolism in the BACHD mouse model of Huntington's disease: Critical role of astrocyte-neuron interactions. J. Cereb. Blood Flow. Metab. 34, 1500–1510.

Brown, M.B., 1975. 400: A Method for Combining Non-Independent, One-Sided Tests of Significance. Biometrics 31, 987–992.

Brozzi, F., Arcuri, C., Giambanco, I., Donato, R., 2009. S100B protein regulates astrocyte shape and migration via interaction with Src kinase. J. Biol. Chem. 284, 8797–8811.

Carter, R.L., Chen, Y., Kunkanjanawan, T., Xu, Y., Moran, S.P., Putkhao, K., Yang, J., Huang, A.H.C., Parnpai, R., Chan, A.W.S., 2014. Reversal of cellular phenotypes in neural cells derived from Huntington's disease monkey-induced pluripotent stem cells. Stem Cell Rep. 3, 585–593.

Castaldo, I., Rosa, De, Romano, M., Zuchegna, A., Squitieri, C., Mechelli, F., Peluso, R., Borrelli, S., Del Mondo, C., Salvatore, E, A., et al., 2019. DNA damage signatures in peripheral blood cells as biomarkers in prodromal huntington disease. Ann. Neurol. 85, 296–301.

Cerutti, S.M., Chadi, G., 2000. S100 immunoreactivity is increased in reactive astrocytes of the visual pathways following a mechanical lesion of the rat occipital cortex. Cell Biol. Int. 24, 35–49.

Cesca, F., Bregant, E., Peterlin, B., Zadel, M., Dubsky De Wittenau, G., Siciliano, G., Ceravolo, R., Petrozzi, L., Pauletto, G., Verriello, L., et al., 2015. Evaluating the SERCA2 and VEGF mRNAs as potential molecular biomarkers of the onset and progression in huntington's disease. PLoS One 10, 1–14.

Chen, L.L., Wu, J.C., Wang, L.H., Wang, J., Qin, Z.H., Difiglia, M., Lin, F., 2012. Rapamycin prevents the mutant huntingtin-suppressed GLT-1 expression in cultured astrocytes. Acta Pharmacol. Sin. 33, 385–392.

Chen, Y., Chen, C.F., Chiang, H.C., Pena, M., Polci, R., Wei, R.L., Edwards, R.A., Hansel, D.E., Chen, P.L., Riley, D.J., 2011b. Mutation of NIMA-related kinase 1 (NEK1) leads to chromosome instability. Mol. Cancer 10, 5.

Chen, Y., Chen, C.F., Riley, D.J., Chen, P.L., 2011a. Nek1 kinase functions in DNA damage response and checkpoint control through a pathway independent of ATM and ATR. Cell Cycle 10, 655–663.

Cho, I.K., Yang, B., Forest, C., Qian, L., Chan, A.W.S., 2019. Amelioration of Huntington's disease phenotype in astrocytes derived from iPSC-derived neural progenitor cells of Huntington's disease monkeys. PLoS One *14*.

Claassen, D.A., Lahue, R.S., 2007. Expansions of CAG•CTG repeats in immortalized human astrocytes. Hum. Mol. Genet. 16, 3088–3096.

Colin, E., Régulier, E., Perrin, V., Dürr, A., Brice, A., Aebischer, P., Déglon, N., Humbert, S., Saudou, F., 2005. Akt is altered in an animal model of Huntington's disease and in patients. Eur. J. Neurosci. 21, 1478–1488.

Conforti, P., Besusso, D., Brocchetti, S., Campus, I., Cappadona, C., Galimberti, M., Laporta, A., Iennaco, R., Rossi, R.L., Dickinson, V.B., et al., 2020. RUES2 hESCs exhibit MGE-biased neuronal differentiation and muHTT-dependent defective specification hinting at SP1. Neurobiol. Dis. 146 (105140).

Dai, H., Leeder, J.S., Cui, Y., 2014. A modified generalized Fisher method for combining probabilities from dependent tests. Front. Genet. 5, 32.

Damiani, C., Rovida, L., Maspero, D., Sala, I., Rosato, L., Di Filippo, M., Pescini, D., Graudenzi, A., Antoniotti, M., Mauri, G., 2020. MaREA4Galaxy: Metabolic reaction enrichment analysis and visualization of RNA-seq data within Galaxy. Comput. Struct. Biotechnol. J. 18, 993–999.

Diaz-Castro, B., Gangwani, M.R., Yu, X., Coppola, G., Khakh, B.S., 2019. Astrocyte molecular signatures in Huntington's disease. Sci. Transl. Med. *11*.

Dvorzhak, A., Vagner, T., Kirmse, K., Grantyn, R., 2016. Functional indicators of glutamate transport in single striatal astrocytes and the influence of Kir4.1 in normal and huntington mice. J. Neurosci. 36, 4959–4975.

Escartin, C., Galea, E., Lakatos, A., O'Callaghan, J.P., Petzold, G.C., Serrano-Pozo, A., Steinhäuser, C., Volterra, A., Carmignoto, G., Agarwal, A., et al., 2021. Reactive astrocyte nomenclature, definitions, and future directions. Nat. Neurosci. 24, 312–325.

Feng, Z., Jin, S., Zupnick, A., Hoh, J., De Stanchina, E., Lowe, S., Prives, C., Levine, A.J., 2006. P53 tumor suppressor protein regulates the levels of Huntingtin gene expression. Oncogene 25, 1–7.

Ferris, H.A., Perry, R.J., Moreira, G.V., Shulman, G.I., Horton, J.D., Kahn, C.R., 2017. Loss of astrocyte cholesterol synthesis disrupts neuronal function and alters whole-body metabolism. Proc. Natl. Acad. Sci. USA 114, 1189–1194.

FitzPatrick, L.M., Hawkins, K.E., Delhove, J.M.K.M., Fernandez, E., Soldati, C., Bullen, L. F., Nohturfft, A., Waddington, S.N., Medina, D.L., Bolaños, J.P., et al., 2018. NF-κB Activity Initiates Human ESC-Derived Neural Progenitor Cell Differentiation by Inducing a Metabolic Maturation Program. Stem Cell Reports 10, 1766–1781.

Garcia, V.J., Rushton, D.J., Tom, C.M., Allen, N.D., Kemp, P.J., Svendsen, C.N., Mattis, V. B., 2019. Huntington's disease patient-derived astrocytes display electrophysiological impairments and reduced neuronal support. Front. Neurosci. 13, 669.

Gaura, V., Lavisse, S., Payoux, P., Goldman, S., Verny, C., Krystkowiak, P., Damier, P., Supiot, F., Bachoud-Levi, A.C., Remy, P., 2017. Association between motor symptoms and brain metabolism in early Huntington disease. JAMA Neurol. 74, 1088–1096.

Gonitel, R., Moffitt, H., Sathasivam, K., Woodman, B., Detloff, P.J., Faull, R.L.M., Bates, G.P., 2008. DNA instability in postmitotic neurons. Proc. Natl. Acad. Sci. USA 105, 3467–3472.

Goold, R., Flower, M., Moss, D.H., Medway, C., Wood-Kaczmar, A., Andre, R., Farshim, P., Bates, G.P., Holmans, P., Jones, L., et al., 2019. FAN1 modifies Huntington's disease progression by stabilizing the expanded HTT CAG repeat. Hum. Mol. Genet. 28, 650–661.

Goold, R., Hamilton, J., Menneteau, T., Flower, M., Bunting, E.L., Aldous, S.G., Porro, A., Vicente, J.R., Allen, N.D., Wilkinson, H., et al., 2021. FAN1 controls mismatch repair complex assembly via MLH1 retention to stabilize CAG repeat expansion in Huntington's disease. Cell Rep. *36*.

Haim, L.Ben, Ceyzériat, K., Sauvage, M.A.C., de, Aubry, F., Auregan, G., Guillermier, M., Ruiz, M., Petit, F., Houitte, D., Faivre, E., et al., 2015. The JAK/STAT3 pathway is a common inducer of astrocyte reactivity in Alzheimer's and Huntington's diseases. J. Neurosci. 35, 2817–2829.

Harada, K., Kamiya, T., Tsuboi, T., 2016. Gliotransmitter release from astrocytes: functional, developmental, and pathological implications in the brain. Front. Neurosci. 9, 1–9.

Hartmann, K., Sepulveda-Falla, D., Rose, I.V.L., Madore, C., Muth, C., Matschke, J., Butovsky, O., Liddelow, S., Glatzel, M., Krasemann, S., 2019. Complement 3+-astrocytes are highly abundant in prion diseases, but their abolishment led to an accelerated disease course and early dysregulation of microglia. Acta Neuropathol. Commun. 7, 83.

Hawkins, B.T., Davis, T.P., 2005. The blood-brain barrier / neurovascular unit in health and disease. Pharmacol. Rev. 57, 173–185.

Hawkins, K.E., Joy, S., Delhove, J.M.K.M., Kotiadis, V.N., Fernandez, E., Fitzpatrick, L. M., Whiteford, J.R., King, P.J., Bolanos, J.P., Duchen, M.R., et al., 2016. NRF2 orchestrates the metabolic shift during induced pluripotent stem cell reprogramming. Cell Rep. 14, 1883–1891.

Higelin, J., Catanese, A., Semelink-Sedlacek, L.L., Oeztuerk, S., Lutz, A.K., Bausinger, J., Barbi, G., Speit, G., Andersen, P.M., Ludolph, A.C., et al., 2018. NEK1 loss-of-function mutation induces DNA damage accumulation in ALS patient-derived motoneurons. Stem Cell Res. 30, 150–162.

Hillen, A.E.J., Burbach, J.P.H., Hol, E.M., 2018. Cell adhesion and matricellular support by astrocytes of the tripartite synapse. Prog. Neurobiol. 165–167, 66–86.

Hodges, A., Strand, A.D., Aragaki, A.K., Kuhn, A., Sengstag, T., Hughes, G., Elliston, L.A., Hartog, C., Goldstein, D.R., Thu, D., et al., 2006. Regional and cellular gene expression changes in human Huntington's disease brain. Hum. Mol. Genet. 15, 965–977.

Hsiao, H.Y., Chen, Y.C., Chen, H.M., Tu, P.H., Chern, Y., 2013. A critical role of astrocyte-mediated nuclear factor-κB-dependent inflammation in huntington's disease. Hum. Mol. Genet. 22, 1826–1842.

Ikeshima-Kataoka, H., 2016. Neuroimmunological implications of AQP4 in astrocytes. Int. J. Mol. Sci. 17, 1–16.

Iyer, R.R., Pluciennik, A., 2021. DNA mismatch repair and its role in Huntington's disease. J. Huntingt. Dis. 10, 75–94.

Jiang, R., Diaz-Castro, B., Looger, L.L., Khakh, B.S., 2016. Dysfunctional calcium and glutamate signaling in striatal astrocytes from Huntington's disease model mice. J. Neurosci. 36, 3453–3470.

Johnson, J., Mercado-Ayón, E., Mercado-Ayón, Y., Dong, Y.N., Halawani, S., Ngaba, L., Lynch, D.R., 2020. Mitochondrial dysfunction in the development and progression of neurodegenerative diseases. Arch. Biochem. Biophys., 108698

Kaminska, B., Gozdz, A., Zawadzka, M., Ellert-Miklaszewska, A., Lipko, M., 2009. MAPK signal transduction underlying brain inflammation and gliosis as therapeutic target. Anat. Rec. 292, 1902–1913.

Kanehisa, M., Goto, S., 2000. KEGG: Kyoto encyclopedia of genes and genomes. Nucleic Acids Res. 28, 27–30.

Karimian, A., Mir, S.M., Parsian, H., Refieyan, S., Mirza-Aghazadeh-Attari, M., Yousefi, B., Majidinia, M., 2019. Crosstalk between phosphoinositide 3-kinase/Akt signaling pathway with DNA damage response and oxidative stress in cancer. J. Cell. Biochem. 120, 10248–10272.

Katz, S., Song, J., Webb, K.P., Lounsbury, N.W., Bryant, C.E., Fraser, I.D.C., 2021. SIGNAL: A web-based iterative analysis platform integrating pathway and network approaches optimizes hit selection from genome-scale assays. Cell Syst *12*, 338–352. e5.

Kerrisk, M.E., Cingolani, L.A., Koleske, A.J., 2014. ECM receptors in neuronal structure, synaptic plasticity, and behavior. Prog. Brain Res. 214, 101–131.
Khakh, B.S., Beaumont, V., Cachope, R., Munoz-Sanjuan, I., Goldman, S.A., Grantyn, R., 2017. Unravelling and exploiting astrocyte dysfunction in Huntington's disease. Trends Neurosci. 40, 422–437.
Kreilaus, F., Spiro, A.S., McLean, C.A., Garner, B., Jenner, A.M., 2016. Evidence for altered cholesterol metabolism in Huntington's disease post mortem brain tissue. Neuropathol. Appl. Neurobiol. 42, 535–546.
Lange, J., Gillham, O., Eaton, S., Ferrari, G., Madej, M., Flower, M., Tedesco, F.S., Muntoni, F., Ferretti, P., 2021b. Dystrophin deficiency affects human astrocyte properties and response to damage. Glia 1–25.
Lange, J., Wood-Kaczmar, A., Ali, A., Farag, S., Ghosh, R., Parker, J., Casey, C., Uno, Y., Kunugi, A., Ferretti, P., et al., 2021a. Mislocalization of nucleocytoplasmic transport proteins in human Huntington's disease PSC-derived striatal neurons. Front. Cell. Neurosci. 15, 1–23.
Langfelder, P., Horvath, S., 2008. WGCNA: an R package for weighted correlation network analysis. BMC Bioinformatics *9*, 559.
Langfelder, P., Mischel, P.S., Horvath, S., 2013. When Is Hub Gene Selection Better than Standard Meta-Analysis? PLoS One *8*.
Lee, E.R., Kim, J.Y., Kang, Y.J., Ahn, J.Y., Kim, J.H., Kim, B.W., Choi, H.Y., Jeong, M.Y., Cho, S.G., 2006. Interplay between PI3K/Akt and MAPK signaling pathways in DNA-damaging drug-induced apoptosis. Biochim. Biophys. Acta Mol. Cell Res. 1763, 958–968.
Liddelow, S.A., Barres, B.A., 2017. Reactive astrocytes: production, function, and therapeutic potential. Immunity 46, 957–967.
Lin, L., Park, J.W., Ramachandran, S., Zhang, Y., Tseng, Y.T., Shen, S., Waldvogel, H.J., Curtis, M.A., Richard, R.L., Troncoso, J.C., et al., 2016. Transcriptome sequencing reveals aberrant alternative splicing in Huntington's disease. Hum. Mol. Genet. 25, 3454–3466.
Love, M.I., Huber, W., Anders, S., 2014. Moderated estimation of fold change and dispersion for RNA-seq data with DESeq2. Genome Biol *15*, 1–21.
Lü, L., Zhang, L., Wai, M.S.M., Yew, D.T.W., Xu, J., 2012. Exocytosis of MTT formazan could exacerbate cell injury. Toxicol. In Vitro 26, 636–644.
Luo, Y., Lin, F.-T., Lin, W.-C., 2004. ATM-mediated stabilization of hMutL DNA mismatch repair proteins augments p53 activation during DNA damage. Mol. Cell. Biol. 24, 6430–6444.
Mächler, P., Wyss, M.T., Elsayed, M., Stobart, J., Gutierrez, R., Von Faber-Castell, A., Kaelin, V., Zuend, M., San Martín, A., Romero-Gómez, I., et al., 2016. In vivo evidence for a lactate gradient from astrocytes to neurons. Cell Metab. 23, 94–102.
Magistretti, P.J., Allaman, I., 2013. Brain energy. Metabolism.
Maiuri, T., Mocle, A.J., Hung, C.L., Xia, J., van Roon-Mom, W.M.C., Truant, R., 2017. Huntingtin is a scaffolding protein in the ATM oxidative DNA damage response complex. Hum. Mol. Genet. 26, 395–406.
Maiuri, T., Suart, C.E., Hung, C.L.K., Graham, K.J., Barba Bazan, C.A., Truant, R., 2019. DNA damage repair in huntington's disease and other neurodegenerative diseases. Neurotherapeutics 16, 948–956.
Martin, W.R.W., Clark, C., Ammann, W., Stoessl, A.J., Shtybel, W., Hayden, M.R., 1992. Cortical glucose metabolism in Huntington's disease. Neurology 42, 223.
Mochel, F., Haller, R.G., 2011. Energy deficit in Huntington disease: why it matters. J. Clin. Investig. 121, 493–499.
Neueder, A., Bates, G.P., 2014. A common gene expression signature in Huntington's disease patient brain regions. BMC Med. Genom. 7, 1–23.
Ooi, J., Langley, S.R., Xu, X., Utami, K.H., Sim, B., Huang, Y., Harmston, N.P., Tay, Y.L., Ziaei, A., Zeng, R., et al., 2019. Unbiased profiling of isogenic Huntington Disease hPSC-derived CNS and peripheral cells reveals strong cell-type specificity of CAG length effects. Cell Rep. 26, 2494–2508 e7.
Palpagama, T.H., Waldvogel, H.J., Faull, R.L.M., Kwakowsky, A., 2019. The role of microglia and astrocytes in Huntington's disease. Front. Mol. Neurosci. 12, 258.
Panier, S., Boulton, S.J., 2014. Double-strand break repair: 53BP1 comes into focus. Nat. Rev. Mol. Cell Biol. 15, 7–18.
Patro, R., Duggal, G., Love, M.I., Irizarry, R.A., Kingsford, C., 2017. Salmon provides fast and bias-aware quantification of transcript expression. Nat. Methods *14*, 417–419.
Pelegrini, A.L., Moura, D.J., Brenner, B.L., Ledur, P.F., Maques, G.P., Henriques, J.A.P., Saffi, J., Lenz, G., 2010. Nek1 silencing slows down DNA repair and blocks DNA damage-induced cell cycle arrest. Mutagenesis 25, 447–454.
Peters, A.C., Young, L.C., Maeda, T., Tron, V.A., Andrew, S.E., 2003. Mammalian DNA mismatch repair protects cells from UVB-induced DNA damage by facilitating apoptosis and p53 activation. DNA Repair 2, 427–435.
Pinto, R.M., Dragileva, E., Kirby, A., Lloret, A., Lopez St., E., Claire, J., Panigrahi, G.B., Hou, C., Holloway, K., Gillis, T., et al., 2013. Mismatch repair genes Mlh1 and Mlh3 modify CAG instability in Huntington's disease mice: genome-wide and candidate approaches. PLoS Genet. *9*.
Podhorecka, M., Skladanowski, A., Bozko, P., 2010. H2AX phosphorylation: its role in DNA damage response and cancer therapy. J. Nucleic Acids 2010.
Polyzos, A.A., Lee, D.Y., Datta, R., Hauser, M., Budworth, H., Holt, A., Mihalik, S., Goldschmidt, P., Frankel, K., Trego, K., et al., 2019. Metabolic reprogramming in astrocytes distinguishes region-specific neuronal susceptibility in huntington mice. Cell Metab. 29 (1258–1273), e11.
Ratovitski, T., Chaerkady, R., Kammers, K., Stewart, J.C., Zavala, A., Pletnikova, O., Troncoso, J.C., Rudnicki, D.D., Margolis, R.L., Cole, R.N., et al., 2016. Quantitative proteomic analysis reveals similarities between Huntington's disease (HD) and Huntington's Disease-Like 2 (HDL2) human brains. J. Proteome Res. 15, 3266–3283.
Rezatabar, S., Karimian, A., Rameshknia, V., Parsian, H., Majidinia, M., Kopi, T.A., Bishayee, A., Sadeghinia, A., Yousefi, M., Monirialamdari, M., et al., 2019. RAS/MAPK signaling functions in oxidative stress, DNA damage response and cancer progression. J. Cell. Physiol. 234, 14951–14965.
Rosas, H.D., Salat, D.H., Lee, S.Y., Zaleta, A.K., Pappu, V., Fischl, B., Greve, D., Hevelone, N., Hersch, S.M., 2008. Cerebral cortex and the clinical expression of Huntington's disease: complexity and heterogeneity. Brain 131, 1057–1068.
Ross, C. a, Tabrizi, S.J., 2011. Huntington's disease: from molecular pathogenesis to clinical treatment. Lancet Neurol. 10, 83–98.
Rueb, U., Vonsattel, JP, H.H., K.H, 2015. The neuropathology of Huntingtoń s disease: classical findings, recent developments and correlation to functional neuroanatomy. Adv. Anat. Embryol. Cell Biol. 217, 1–146.
Schmittgen, T.D., Livak, K.J., 2008. Analyzing real-time PCR data by the comparative CT method. Nat. Protoc. 3, 1101–1108.
Shelbourne, P.F., Keller-McGandy, C., Bi, W.L., Yoon, S.R., Dubeau, L., Veitch, N.J., Vonsattel, J.P., Wexler, N.S., Norman, A., Augood, S.J., 2007. Triplet repeat mutation length gains correlate with cell-type specific vulnerability in Huntington disease brain. Hum. Mol. Genet. 16, 1133–1142.
Shin, H., Kim, M.H., Lee, S.J., Lee, K.H., Kim, M.J., Kim, J.S., Cho, J.W., 2013. Decreased metabolism in the cerebral cortex in early-stage huntington's disease: a possible biomarker of disease progression? J. Clin. Neurol. 9, 21–25.
Singh, A., Abraham, W.C., 2017. Astrocytes and synaptic plasticity in health and disease. Exp. Brain Res. 235, 1645–1655.
Skene, D.J., Middleton, B., Fraser, C.K., Pennings, J.L.A., Kuchel, T.R., Rudiger, S.R., Bawden, C.S., Morton, A.J., 2017. Metabolic profiling of presymptomatic Huntington's disease sheep reveals novel biomarkers. Sci. Rep. 7, 1–16.
Soneson, C., Love, M.I., Robinson, M.D., 2016. Differential analyses for RNA-seq: Transcript-level estimates improve gene-level inferences. F1000Research *4*, 1–23.
Swami, M., Hendricks, A.E., Gillis, T., Massood, T., Mysore, J., Myers, R.H., Wheeler, V. C., 2009. Somatic expansion of the Huntington's disease CAG repeat in the brain is associated with an earlier age of disease onset. Hum. Mol. Genet. 18, 3039–3047.
Tidball, A.M., Neely, M.D., Chamberlin, R., Aboud, A.A., Kumar, K.K., Han, B., Bryan, M. R., Aschner, M., Ess, K.C., Bowman, A.B., 2016. Genomic instability associated with p53 knockdown in the generation of Huntington's disease human induced pluripotent stem cells. PLoS One *11*.
Tong, X., Ao, Y., Faas, G.C., Nwaobi, S.E., Xu, J., Haustein, M.D., Anderson, M.A., Mody, I., Olsen, M.L., Sofroniew, M.V., et al., 2014. Astrocyte Kir4.1 ion channel deficits contribute to neuronal dysfunction in Huntington's disease model mice. Nat. Neurosci. 17, 694–703.
Vagaska, B., Gillham, O., Ferretti, P., 2020. Modelling human CNS injury with human neural stem cells in 2- and 3-Dimensional cultures. Sci. Rep. 10, 1–14.
Vainchtein, I.D., Molofsky, A.V., 2020. Astrocytes and microglia: in sickness and in health. Trends Neurosci. 43, 144–154.
Valavanidis, A., Vlachogianni, T., Fiotakis, C., 2009. 8-Hydroxy-2′ -deoxyguanosine (8-OHdG): a critical biomarker of oxidative stress and carcinogenesis. J. Environ. Sci. Health Part C Environ. Carcinog. Ecotoxicol. Rev. 27, 120–139.
Valenza, M., Leoni, V., Karasinska, J.M., Petricca, L., Fan, J., Carroll, J., Pouladi, M.A., Fossale, E., Nguyen, H.P., Riess, O., et al., 2010. Cholesterol defect is marked across multiple rodent models of Huntington's disease and is manifest in astrocytes. J. Neurosci. 30, 10844–10850.
Valenza, M., Marullo, M., Di Paolo, E., Cesana, E., Zuccato, C., Biella, G., Cattaneo, E., 2015. Disruption of astrocyte-neuron cholesterol cross talk affects neuronal function in Huntington's disease. Cell Death Differ. 22, 690–702.
Vonsattel, J.P., Myers, R.H., Stevens, T.J., Ferrante, R.J., Bird, E.D., Richardson, E.P., 1985. Neuropathological classification of huntington's disease. J. Neuropathol. Exp. Neurol. 44, 559–577.
Wilson, D.J., 2019. The harmonic mean p-value for combining dependent tests. Proc. Natl. Acad. Sci. U. S. A. 116, 1195–1200.
Wójtowicz, A.M., Dvorzhak, A., Semtner, M., Grantyn, R., 2013. Reduced tonic inhibition in striatal output neurons from Huntington mice due to loss of astrocytic GABA release through GAT-3. Front. Neural Circuits 7, 1–12.
Xie, Z., Smith, C.J., Van Eldik, L.J., 2004. Activated glia induce neuron death via MAP kinase signaling pathways involving JNK and p38. Glia 45 (170–179).
Xiong, Y., Sun, S., Teng, S., Jin, M., Zhou, Z., 2018. Ca2+-dependent and Ca2+-independent ATP release in astrocytes. Front. Mol. Neurosci. 11, 1–5.